

ANISOTROPIC POLYGONAL AND POLYHEDRAL DISCRETIZATIONS IN FINITE ELEMENT ANALYSIS

STEFFEN WEISSER

ABSTRACT. New interpolation and quasi-interpolation operators of Clément- and Scott-Zhang-type are analyzed on anisotropic polygonal and polyhedral meshes. Since no reference element is available, an appropriate linear mapping to a reference configuration plays a crucial role. A priori error estimates are derived respecting the anisotropy of the discretization. Finally, the found estimates are employed to propose an adaptive mesh refinement based on bisection which leads to highly anisotropic and adapted discretizations with general element shapes in two- and three-dimensions.

1. INTRODUCTION

In nowadays computer simulations the use of highly adapted meshes for the treatment of partial differential equations is crucial in order to achieve accurate and efficient results. The adaptive Finite Element Method (FEM) is a well-founded and accepted strategy which reduces the computational cost while improving the accuracy of the approximation. When dealing with highly anisotropic solutions of boundary value problems, it is widely recognized that anisotropic mesh refinements have significant potential for improving the efficiency of the solution process. Pioneering works for the analysis of Finite Element Methods on anisotropic meshes have been performed by Apel [2] as well as by Formaggia and Perotto [11, 12]. The meshes usually consist of triangular and quadrilateral elements in two-dimension as well as on tetrahedral and hexahedral elements in three-dimension. First results on a posteriori error estimates for driving adaptive mesh refinement with anisotropic elements have been derived by Kunert [18] for triangular and tetrahedral meshes. For the mesh generation and adaptation different concepts are available which rely on metric-based strategies, see, e.g., [15, 19], or on splitting of elements, see [22] and the references therein. The anisotropic splitting of classical elements, however, results in certain restrictions why several authors combine this approach with additional strategies like edge swapping, node removal and local node movement. These restrictions come from the limited element shapes and the necessity to remove or handle hanging nodes in the discretization. For three-dimensional elements the situation is even more difficult. In order to relax the admissibility of the meshes one can apply discontinuous Galerkin (DG) methods, see [13], but consequently the conformity of the approximations is lost.

In recent years the attraction of polytopal meshes increased in the discretization of boundary value problems. These meshes consist of polygonal and polyhedral elements in two- and three-dimensions, respectively, and find their applications in polygonal FEM [24], mimetic discretizations [4] as well as in the BEM-based

2010 *Mathematics Subject Classification.* 65D05, 65N15, 65N30, 65N50.

Key words and phrases. anisotropic finite elements, polyhedral mesh, interpolation, error estimate, mesh adaptation.

FEM [9], where BEM stands for Boundary Element Method, and the Virtual Element Method (VEM) [3]. One of the promising features is the high flexibility of the element shapes in the discretization. Since the elements may contain an arbitrary number of nodes on their boundary, the notion of “hanging nodes” is naturally included in most of the previously mentioned approaches. A posteriori error estimates have been developed for the BEM-based FEM as well as for the VEM and they have been successfully applied in adaptive mesh refinement strategies, see [5, 6, 7, 26, 28, 29].

To the best of our knowledge, the polytopal elements have to fulfil some kind of isotropy in all previous publications, i.e., anisotropic elements, which are very thin and elongated, are explicitly excluded from the error analysis. Since such anisotropic polytopal elements promise a high potential in the accurate resolution of sharp layers in the solutions of boundary value problems due to their enormous flexibility, we develop an appropriate framework in this article. Geometric information is used in order to characterize the anisotropy of the elements and to give a definition of mesh regularity in a more general sense. In this article, we address the approximation space coming from the BEM-based FEM and the VEM in two- and three-dimensions, but the ideas are also applicable to polygonal FEM [24] with harmonic or other generalized barycentric coordinates, see [10, 17] and the references therein. We study interpolation as well as quasi-interpolation operators and derive a priori interpolation error estimates that can be applied in the analysis of BEM-based FEM and VEM after the use of Céa- or Strang-type lemmata. The derived estimates are further used to steer an anisotropic mesh refinement procedure in which polytopal elements are bisected successively. Numerical experiments demonstrate the flexibility and the potential for highly anisotropic polytopal discretizations.

The article is organized as follows: Section 2 introduces the approximation space and discusses the regularity as well as the properties of anisotropic polytopal meshes. In Section 3, an anisotropic trace inequality is derived and best approximation results are proved. Quasi-interpolation operators of Clément- and Scott-Zhang-type are introduced and analyzed in Section 4. The derived framework is applied to pointwise interpolation in Section 5. Finally, numerical experiments are performed with a new anisotropic mesh refinement strategy in Section 6 and some conclusions are drawn in Section 7.

2. POLYTOPAL MESHES AND DISCRETIZATION

Let $\Omega \subset \mathbb{R}^d$ be a bounded polytopal domain in two or three space dimensions and let \mathcal{K}_h be a decomposition of Ω into non-overlapping polytopal elements, such that

$$\bar{\Omega} = \bigcup_{K \in \mathcal{K}_h} \bar{K}.$$

For $d = 2$, each polygonal element K consists of nodes and straight edges which are always situated between two nodes. In three space dimensions ($d = 3$), the boundary ∂K of a polyhedral element K is formed by flat polygonal faces which are again framed by edges and nodes. In the context of polytopal meshes it is explicitly allowed that the dihedral angles of adjacent faces and the angles of neighbouring edges are equal to π . Thus, the notion of hanging nodes and edges in classical finite element methods is naturally included in polytopal meshes and does not result in any restrictions.

In order to treat the two- and three-dimensional case in the following simultaneously, we denote the $d - 1$ dimensional objects, i.e. the edges ($d = 2$) and the faces ($d = 3$), by E and the set of all of them by \mathcal{E}_h . The nodes in the discretization are denoted by \mathbf{x}_i , $i = 1, \dots, N$, and the indices of the nodes belonging to $K \in \mathcal{K}_h$ and $E \in \mathcal{E}_h$ are given by the sets $I(K)$ and $I(E)$, respectively.

We make use of the usual space of square integrable functions $L_2(\omega)$ and the Sobolev Spaces $H^k(\omega)$, $k = 1, 2$ and denote their norms by $\|\cdot\|_{L_2(\omega)}$ and $\|\cdot\|_{H^k(\omega)}$, respectively, where $\omega \subset \bar{\Omega}$ is a d or $d - 1$ dimensional domain, see [1]. The inner product of $L_2(\omega)$ is written as $(\cdot, \cdot)_{L_2(\omega)}$ and the semi-norm in $H^k(\omega)$ as $|\cdot|_{H^k(\omega)}$.

2.1. Finite dimensional discretization of the function space. The discrete function space considered in this publication originates from the BEM-based Finite Element Method [26] and the Virtual Element Method [3]. For $d = 2$, we have

$$V_h = \{v \in H^1(\Omega) : \Delta v|_K = 0 \forall K \in \mathcal{K}_h \text{ and } v|_E \text{ linear } \forall E \in \mathcal{E}_h\}.$$

In the two-dimensional case the basis functions of V_h are also known as generalized barycentric coordinates under the name harmonic coordinates, see [17]. This nodal basis can be constructed as

$$(1) \quad \begin{aligned} -\Delta \psi_i &= 0 \quad \text{in } K, \quad \forall K \in \mathcal{K}_h, \\ \psi_i(\mathbf{x}_j) &= \delta_{ij} \quad \text{for } j = 1, \dots, N, \\ \psi_i &\text{ linear on each edge,} \end{aligned}$$

for $i = 1, \dots, N$. Each basis function ψ_i is thus the solution of a local boundary value problem over each element $K \in \mathcal{K}_h$. For $d = 3$ this definition generalizes according to [21] to

$$V_h = \{v \in H^1(\Omega) : \Delta v|_K = 0 \forall K \in \mathcal{K}_h \text{ and } v|_E \in V_h(E) \forall E \in \mathcal{E}_h\},$$

where $V_h(E)$ denotes the two-dimensional discretization space over the face E . The nodal basis functions are constructed as in (1) but they have to fulfil additionally the Laplace equation in the linear parameter space of each face. Depending on the shapes of the elements and faces, the Laplace equations might be understood in a weak sense. Since $v \in H^1(K)$ locally and due to the continuity of v across edges and faces for $v \in V_h$, the conformity $V_h \subset H^1(\Omega)$ follows. A further adaptation of the approximation space in three-dimensions can be found in [14]. In order to achieve good approximation properties in V_h the polytopal mesh and the elements in particular have to fulfil certain regularity assumptions.

2.2. Characterisation of anisotropy and affine mapping. Let $K \subset \mathbb{R}^d$, $d = 2, 3$ be a bounded polytopal element. Furthermore, we assume that K is not degenerated, i.e. $|K| = \text{meas}_d(K) > 0$. Then, we define the center or mean of K as

$$\bar{\mathbf{x}}_K = \frac{1}{|K|} \int_K \mathbf{x} \, d\mathbf{x}$$

and the covariance matrix of K as

$$M_{\text{Cov}}(K) = \frac{1}{|K|} \int_K (\mathbf{x} - \bar{\mathbf{x}}_K)(\mathbf{x} - \bar{\mathbf{x}}_K)^\top \, d\mathbf{x} \in \mathbb{R}^{d \times d}.$$

Obviously, M_{Cov} is real valued, symmetric and positive definite since K is not degenerated. Therefore, it admits an eigenvalue decomposition

$$M_{\text{Cov}}(K) = U_K \Lambda_K U_K^\top$$

with

$$U^\top = U^{-1} \quad \text{and} \quad \Lambda_K = \text{diag}(\lambda_{K,1}, \dots, \lambda_{K,d}).$$

Without loss of generality we assume that the eigenvalues fulfil $\lambda_{K,1} \geq \dots \geq \lambda_{K,d} > 0$ and that the eigenvectors $\mathbf{u}_{K,1}, \dots, \mathbf{u}_{K,d}$ collected in U are oriented in the same way for all considered elements $K \in \mathcal{K}_h$.

The eigenvectors of $M_{\text{Cov}}(K)$ give the characteristic directions of K . This fact is, e.g., also used in the principal component analysis (PCA). The eigenvalue $\lambda_{K,j}$ is the variance of the underlying data in the direction of the corresponding eigenvector $\mathbf{u}_{K,j}$. Thus, the square root of the eigenvalues give the standard deviations in a statistical setting. Consequently, if

$$M_{\text{Cov}}(K) = cI$$

for $c > 0$, there are no dominant directions in the element K . We can characterise the anisotropy with the help of the quotient $\lambda_{K,1}/\lambda_{K,d} \geq 1$ and call an element

$$\text{isotropic, if } \frac{\lambda_{K,1}}{\lambda_{K,d}} \approx 1,$$

$$\text{and anisotropic, if } \frac{\lambda_{K,1}}{\lambda_{K,d}} \gg 1.$$

We might even characterise for $d = 3$ whether the element is anisotropic in one or more directions by comparing the different combinations of eigenvalues.

Exploiting the spectral information of the polytopal elements, we next introduce a linear transformation of an anisotropic element K onto a kind of reference element \widehat{K} . For each $\mathbf{x} \in K$, we define the mapping by

$$(2) \quad \mathbf{x} \mapsto \widehat{\mathbf{x}} = F_K(\mathbf{x}) = A_K \mathbf{x} \quad \text{with} \quad A_K = \alpha_K \Lambda_K^{-1/2} U_K^\top,$$

and $\alpha > 0$, which will be chosen later. $\widehat{K} = F_K(K)$ is called reference configuration later on.

Lemma 1. *Under the above transformation, it holds*

- (i) $|\widehat{K}| = |K| |\det(A_K)| = \alpha^d |K| / \sqrt{\prod_{j=1}^d \lambda_{K,j}}$,
- (ii) $\bar{\mathbf{x}}_{\widehat{K}} = F_K(\bar{\mathbf{x}}_K)$,
- (iii) $M_{\text{Cov}}(\widehat{K}) = \alpha^2 I$.

Proof. First, we recognize that

$$\det(A_K) = \alpha^d \det(\Lambda_K^{-1/2} U_K^\top) = \alpha^d / \sqrt{\det(\Lambda_K)} = \alpha^d / \sqrt{\prod_{j=1}^d \lambda_{K,j}}.$$

Consequently, we obtain by the transformation

$$|\widehat{K}| = \int_{\widehat{K}} d\widehat{\mathbf{x}} = |K| |\det(A_K)| = \alpha^d |K| / \sqrt{\det(M_{\text{Cov}}(K))},$$

that proves the first statement. For the center, we have

$$\bar{\mathbf{x}}_{\widehat{K}} = \frac{1}{|\widehat{K}|} \int_{\widehat{K}} \widehat{\mathbf{x}} d\widehat{\mathbf{x}} = \frac{|\det(A_K)|}{|\widehat{K}|} A_K \int_K \mathbf{x} d\mathbf{x} = A_K \bar{\mathbf{x}}_K.$$

The covariance matrix has the form

$$\begin{aligned}
M_{\text{Cov}}(\widehat{K}) &= \frac{1}{|\widehat{K}|} \int_{\widehat{K}} (\widehat{\mathbf{x}} - \bar{\mathbf{x}}_{\widehat{K}})(\widehat{\mathbf{x}} - \bar{\mathbf{x}}_{\widehat{K}})^\top d\widehat{\mathbf{x}} \\
&= \frac{|\det(A_K)|}{|\widehat{K}|} \int_K A_K(\mathbf{x} - \bar{\mathbf{x}}_K)(A_K(\mathbf{x} - \bar{\mathbf{x}}_K))^\top d\mathbf{x} \\
&= A_K M_{\text{Cov}}(K) A_K^\top \\
&= \alpha^2 (\Lambda_K^{-1/2} U_K^\top) (U_K \Lambda_K U_K^\top) (\Lambda_K^{-1/2} U_K^\top)^\top \\
&= \alpha^2 I,
\end{aligned}$$

that finishes the proof. \square

According to the previous lemma, the reference configuration \widehat{K} is isotropic, since $\lambda_{\widehat{K},1}/\lambda_{\widehat{K},d} = 1$, and thus, it has no dominant direction. We can still choose the parameter α in the mapping. We might use $\alpha = 1$ such that the variance of the element in every direction is equal to one. On the other hand, we can use the parameter α in order to normalise the volume of \widehat{K} such that $|\widehat{K}| = 1$. This is achieved by

$$(3) \quad \alpha_K = \left(\frac{\sqrt{\det(M_{\text{Cov}}(K))}}{|K|} \right)^{1/d} = \left(\frac{\sqrt{\prod_{j=1}^d \lambda_{K,j}}}{|K|} \right)^{1/d},$$

see Lemma 1, and will be used in the rest of the paper.

Example 1. The transformation (2) for α according to (3) is demonstrated for an anisotropic element $K \subset \mathbb{R}^2$, i.e. $d = 2$. The element K is depicted in Fig. 1 (left). The eigenvalues of $M_{\text{Cov}}(K)$ are

$$\lambda_{K,1} \approx 3.37 \cdot 10^1 \quad \text{and} \quad \lambda_{K,2} \approx 1.69 \cdot 10^{-1},$$

and thus

$$\frac{\lambda_{K,1}}{\lambda_{K,2}} \approx 1.99 \cdot 10^2 \gg 1.$$

In Fig. 1, we additionally visualize the eigenvectors of $M_{\text{Cov}}(K)$ scaled by the square root of their corresponding eigenvalue and centered at the mean of the element. The ellipse is the one given uniquely by the scaled vectors. In the right picture of Fig. 1, the transformed element $\widehat{K} = F_K(K)$ is given with the scaled eigenvectors of its covariant matrix $M_{\text{Cov}}(\widehat{K})$. The computation verify $|\widehat{K}| = 1$, and we have

$$M_{\text{Cov}}(\widehat{K}) \approx \begin{pmatrix} 8.68 \cdot 10^{-2} & 5.49 \cdot 10^{-16} \\ 5.49 \cdot 10^{-16} & 8.68 \cdot 10^{-2} \end{pmatrix}.$$

2.3. Regular isotropic and anisotropic polytopal meshes. In view of the quasi-interpolation and interpolation operators and their approximation properties, we state the mesh requirements for their analysis. For the regularity of usual isotropic meshes we refer to [21, 27]. However, these assumptions are rather standard, see also [3].

Definition 1 (regular (isotropic) mesh). Let \mathcal{K}_h be a polytopal mesh. \mathcal{K}_h is called *regular* or a *regular isotropic mesh*, if all elements $K \in \mathcal{K}_h$ fulfil:

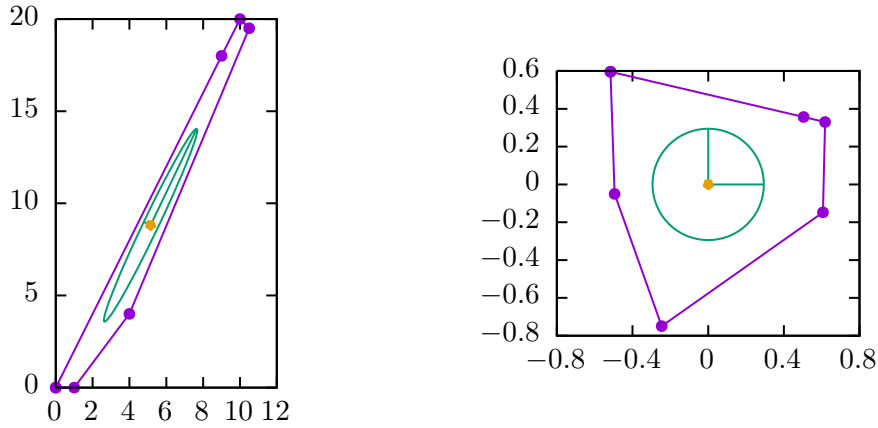


FIGURE 1. Demonstration of transformation (2): original anisotropic element (left) and transformed element centered at the origin (right)

- (i) K is a star-shaped polygon/polyhedron with respect to a circle/ball of radius ρ_K and midpoint \mathbf{z}_K .
- (ii) Their aspect ratio is uniformly bounded from above by σ_K , i.e. $h_K/\rho_K < \sigma_K$.
- (iii) For the element K and all its edges $e \subset \partial K$ it holds $h_K \leq c_K|e|$, where $|e|$ is the edge length.
- (iv) In the case $d = 3$, all polygonal faces $E \subset \partial K$ of the polyhedral element K are star-shaped with respect to a circle of radius ρ_E and midpoint \mathbf{z}_E and their aspect ratio is uniformly bounded, i.e. $h_E/\rho_E < \sigma_E$.

In [27], it has been shown that under these assumptions, the triangulation of a regular polygon K , see Fig. 2, obtained by connecting its nodes with the point \mathbf{z}_K is shape-regular in the sense of Ciarlet. The same holds for regular polyhedral elements. A discretization into tetrahedra is constructed by connecting the nodes of each face $E \subset \partial K$ with \mathbf{z}_E , see Fig. 2, and by connecting the vertices of the obtained triangles on ∂K with the midpoint \mathbf{z}_K . This tetrahedral decomposition of K is shape-regular in the usual sense, see [21]. Furthermore, it can be shown that the number of nodes on the boundary of K is uniformly bounded, cf. [28]. Consequently, the number of simplices in the auxiliary triangulation into triangles ($d = 2$) and tetrahedra ($d = 3$) is also uniformly bounded.

In the definition of regular anisotropic meshes, we make use of the previously introduced reference configuration.

Definition 2 (regular anisotropic mesh). Let \mathcal{K}_h be a polytopal mesh with anisotropic elements. \mathcal{K}_h is called a *regular anisotropic mesh*, if

- (i) The reference configuration \widehat{K} for all $K \in \mathcal{K}_h$ obtained by (2) is a regular polytopal element according to Definition 1.
- (ii) Neighbouring elements behave similarly in their anisotropy. More precisely, for two neighbouring elements K_1 and K_2 , i.e. $\overline{K_1} \cap \overline{K_2} \neq \emptyset$, with covariance matrices

$$M_{\text{Cov}}(K_1) = U_{K_1} \Lambda_{K_1} U_{K_1}^\top \quad \text{and} \quad M_{\text{Cov}}(K_2) = U_{K_2} \Lambda_{K_2} U_{K_2}^\top$$

as defined above, we can write

$$\Lambda_{K_2} = (I + \Delta^{K_1, K_2}) \Lambda_{K_1} \quad \text{and} \quad U_{K_2} = R^{K_1, K_2} U_{K_1}$$

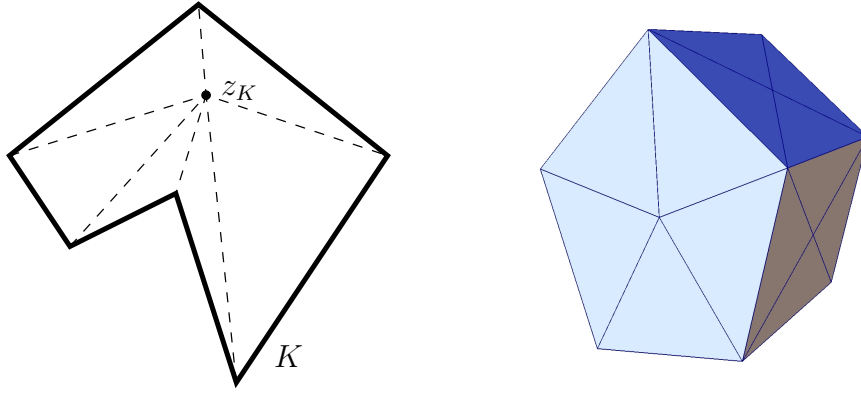


FIGURE 2. Auxiliary triangulation of regular element K for $d = 2$ into triangles (left) and for $d = 3$ into tetrahedra (right)

with

$$\Delta^{K_1, K_2} = \text{diag} \left(\delta_j^{K_1, K_2} : j = 1, \dots, d \right),$$

and a rotation matrix $R^{K_1, K_2} \in \mathbb{R}^{d \times d}$ such that for $j = 1, \dots, d$

$$0 \leq |\delta_j^{K_1, K_2}| < c_\delta < 1 \quad \text{and} \quad 0 \leq \|R^{K_1, K_2} - I\|_2 \left(\frac{\lambda_{K_1, 1}}{\lambda_{K_1, d}} \right)^{1/2} < c_R$$

uniformly for all neighbouring elements, where $\|\cdot\|_2$ denotes the spectral norm.

In the rest of the paper, c denotes a generic constant which depends on the regularity parameters of the mesh $(\sigma_{\mathcal{K}}, c_{\mathcal{K}}, \sigma_{\mathcal{E}}, c_\delta, c_R)$ and the space dimension d .

Remark 1. For $d = 2$, the rotation matrix has the form

$$R^{K_1, K_2} = \begin{pmatrix} \cos \phi^{K_1, K_2} & -\sin \phi^{K_1, K_2} \\ \sin \phi^{K_1, K_2} & \cos \phi^{K_1, K_2} \end{pmatrix},$$

with an angle ϕ^{K_1, K_2} . For the spectral norm $\|R^{K_1, K_2} - I\|_2$, we recognize that

$$(R^{K_1, K_2} - I)^\top (R^{K_1, K_2} - I) = (\sin^2 \phi^{K_1, K_2} + (1 - \cos \phi^{K_1, K_2})^2) I,$$

and consequently

$$\begin{aligned} \|R^{K_1, K_2} - I\|_2 &= (\sin^2 \phi^{K_1, K_2} + (1 - \cos \phi^{K_1, K_2})^2)^{1/2} \\ &= 2 \left| \sin \left(\frac{\phi^{K_1, K_2}}{2} \right) - \sin(0) \right| \\ &\leq |\phi^{K_1, K_2}|, \end{aligned}$$

according to the mean value theorem. The assumption on the spectral norm in Definition 2 can thus be replaced by

$$|\phi^{K_1, K_2}| \left(\frac{\lambda_{K_1, 1}}{\lambda_{K_1, 2}} \right)^{1/2} < c_\phi.$$

This implies that neighbouring highly anisotropic elements has to be aligned in almost the same directions, whereas isotropic or moderately anisotropic elements might vary in their characteristic directions locally.

Let us study the reference configuration $\widehat{K} \subset \mathbb{R}^d$, $d = 2, 3$ of $K \in \mathcal{K}_h$, which is regular. Due to the scaling with α_K , it is $|\widehat{K}| = 1$ and we obtain

$$1 = |\widehat{K}| \leq h_{\widehat{K}}^d \leq \sigma_{\mathcal{K}}^d \rho_{\widehat{K}}^d = \sigma_{\mathcal{K}}^d \nu \pi \rho_{\widehat{K}}^d / (\nu \pi) \leq \sigma_{\mathcal{K}}^d |\widehat{K}| / (\nu \pi) = \sigma_{\mathcal{K}}^d / (\nu \pi),$$

where $\nu = 1$ for $d = 2$ and $\nu = 4/3$ for $d = 3$, since the circle/ball is inscribed the element \widehat{K} . Consequently, we obtain

$$(4) \quad 1 \leq h_{\widehat{K}} \leq \frac{\sigma_{\mathcal{K}}}{(\nu \pi)^{1/d}}.$$

Furthermore, for $d = 3$, let \widehat{E} be a face of \widehat{K} and denote by \widehat{e} one of its edges $\widehat{e} \subset \partial \widehat{E}$. Due to the regularity, we find

$$|\widehat{E}| \geq \pi \rho_{\widehat{E}}^2 \geq \pi h_{\widehat{E}}^2 / \sigma_{\widehat{E}}^2 \geq \pi h_{\widehat{e}}^2 / \sigma_{\widehat{e}}^2 \geq \pi h_{\widehat{K}}^2 / (c_{\mathcal{K}} \sigma_{\widehat{E}}^2),$$

and thus for $d = 2, 3$

$$(5) \quad h_{\widehat{K}}^{d-1} \leq c |\widehat{E}|.$$

A regular anisotropic element can be mapped according to the previous definition onto a regular polytopal element in the usual sense. In the definition of quasi-interpolation operators, we deal, however, with patches of elements instead of single elements. Thus, we study the mapping of such patches. Let ω_i be the neighbourhood of the node \mathbf{x}_i which is defined by

$$\bar{\omega}_i = \bigcup \{ \overline{K'} : \mathbf{x}_i \in \overline{K'}, \quad K' \in \mathcal{K}_h \}.$$

The neighbourhood ω_i is also described by

$$\bar{\omega}_i = \text{supp } \psi_i,$$

where ψ_i is the nodal basis function in V_h corresponding to \mathbf{x}_i . Furthermore, the neighbourhoods ω_E and ω_K of edges/faces E and elements K are considered. They are given by

$$\bar{\omega}_E = \bigcup_{i \in I(E)} \bar{\omega}_i \quad \text{and} \quad \bar{\omega}_K = \bigcup_{i \in I(K)} \bar{\omega}_i.$$

Lemma 2. *Let \mathcal{K}_h be a regular anisotropic mesh, ω_i be a patch as described above, and $K_1, K_2 \in \mathcal{K}_h$ with $K_1, K_2 \subset \omega_i$. The mapped element $F_{K_1}(K_2)$ is regular in the sense of Definition 1 with slightly perturbed regularity parameters $\tilde{\sigma}_{\mathcal{K}}$ and $\tilde{c}_{\mathcal{K}}$ depending only on the regularity of \mathcal{K}_h . Consequently, the mapped patch $F_K(\omega_i)$ consists of regular polytopal elements for all $K \in \mathcal{K}_h$ with $K \subset \omega_i$.*

Proof. We verify Definition 1 for the mapped element $\tilde{K}_2 = F_{K_1}(K_2)$.

First, we address (i) of Definition 1. $\widehat{K}_2 = F_{K_2}(K_2)$ is regular and thus, star-shaped with respect to a circle/ball \widehat{B} . If we transform \widehat{K}_2 into \tilde{K}_2 with the mapping $F_{K_1} \circ F_{K_2}^{-1}$, see Fig. 3, the circle/ball \widehat{B} is transformed into an ellipse/ellipsoid $\tilde{B} = F_{K_1} \circ F_{K_2}^{-1}(\widehat{B})$. Since the transformations are linear, the element \tilde{K}_2 is star-shaped with respect to the ellipse/ellipsoid \tilde{B} and in particular with respect to the circle/ball inscribed \tilde{B} .

Next, we address (ii) of Definition 1 and we bound the aspect ratio. The radius $\rho_{\tilde{K}_2}$ of the inscribed circle/ball as above is equal to the smallest semi-axis of

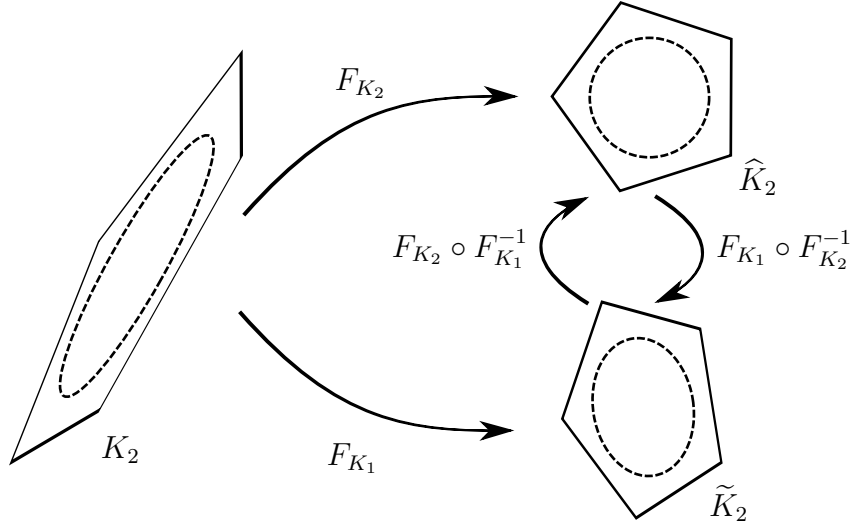


FIGURE 3. Anisotropic element K_2 with mapped regular element \widehat{K}_2 and perturbed mapped element $\widetilde{K}_2 = F_{K_1}(K_2)$

the ellipse/ellipsoid \widetilde{B} . Let $\widetilde{\mathbf{x}}_1$ and $\widetilde{\mathbf{x}}_2$ be the intersection of \widetilde{B} and the inscribed circle/ball. Thus, we obtain

$$\begin{aligned}
2\rho_{\widehat{K}_2} &= |F_{K_2} \circ F_{K_1}^{-1}(\widetilde{\mathbf{x}}_1 - \widetilde{\mathbf{x}}_2)| \\
&= \left| \alpha_{K_2} \Lambda_{K_2}^{-1/2} U_{K_2}^\top \frac{1}{\alpha_{K_1}} U_{K_1} \Lambda_{K_1}^{1/2} (\widetilde{\mathbf{x}}_1 - \widetilde{\mathbf{x}}_2) \right| \\
&= \frac{\alpha_{K_2}}{\alpha_{K_1}} \left| \Lambda_{K_1}^{-1/2} (I + \Delta^{K_1, K_2})^{-1/2} U_{K_1}^\top (R^{K_1, K_2})^\top U_{K_1} \Lambda_{K_1}^{1/2} (\widetilde{\mathbf{x}}_1 - \widetilde{\mathbf{x}}_2) \right| \\
&= \frac{\alpha_{K_2}}{\alpha_{K_1}} \left| (I + \Delta^{K_1, K_2})^{-1/2} \left(\Lambda_{K_1}^{-1/2} U_{K_1}^\top (R^{K_1, K_2} - I)^\top U_{K_1} \Lambda_{K_1}^{1/2} + I \right) (\widetilde{\mathbf{x}}_1 - \widetilde{\mathbf{x}}_2) \right| \\
&\leq \frac{\alpha_{K_2}}{\alpha_{K_1}} \left\| (I + \Delta^{K_1, K_2})^{-1/2} \right\|_2 \left(\left\| \Lambda_{K_1}^{-1/2} \right\|_2 \left\| R^{K_1, K_2} - I \right\|_2 \left\| \Lambda_{K_1}^{1/2} \right\|_2 + 1 \right) 2\rho_{\widetilde{K}_2} \\
&= \frac{\alpha_{K_2}}{\alpha_{K_1}} \max_{j=1, \dots, d} \left\{ (1 + \delta_j^{K_1, K_2})^{-1/2} \right\} \left(1 + \left(\frac{\lambda_{K_1, 1}}{\lambda_{K_1, d}} \right)^{1/2} \left\| R^{K_1, K_2} - I \right\|_2 \right) 2\rho_{\widetilde{K}_2},
\end{aligned}$$

since the spectral norm $\|\cdot\|_2$ is invariant under rotations, and U_{K_1} is such a rotation. With similar arguments, we can bound $h_{\widetilde{K}_2}$. Therefore, let $\widetilde{\mathbf{x}}_1, \widetilde{\mathbf{x}}_2 \in \partial\widetilde{K}_2$ be such that $h_{\widetilde{K}_2} = |\widetilde{\mathbf{x}}_1 - \widetilde{\mathbf{x}}_2|$ and $\widehat{\mathbf{x}}_i = F_{K_2} \circ F_{K_1}^{-1}(\widetilde{\mathbf{x}}_i) \in \partial\widehat{K}_2$, $i = 1, 2$. With similar considerations as above, we obtain

$$\begin{aligned}
h_{\widetilde{K}_2} &= |F_{K_1} \circ F_{K_2}^{-1}(\widehat{\mathbf{x}}_1 - \widehat{\mathbf{x}}_2)| \\
&\leq \frac{\alpha_{K_1}}{\alpha_{K_2}} \max_{j=1, \dots, d} \left\{ (1 + \delta_j^{K_1, K_2})^{1/2} \right\} \left(1 + \left(\frac{\lambda_{K_1, 1}}{\lambda_{K_1, d}} \right)^{1/2} \left\| R^{K_1, K_2} - I \right\|_2 \right) h_{\widehat{K}_2}.
\end{aligned}$$

Exploiting the last two estimates yields

$$\begin{aligned} \frac{h_{\tilde{K}_2}}{\rho_{\tilde{K}_2}} &\leq \frac{\max_{j=1,\dots,d} \sqrt{1 + \delta_j^{K_1, K_2}}}{\min_{j=1,\dots,d} \sqrt{1 + \delta_j^{K_1, K_2}}} \left(1 + \left(\frac{\lambda_{K_1,1}}{\lambda_{K_1,d}} \right)^{1/2} \|R^{K_1, K_2} - I\|_2 \right)^2 \frac{h_{\hat{K}_2}}{\rho_{\hat{K}_2}} \\ &\leq \sqrt{\frac{1 + c_\delta}{1 - c_\delta}} (1 + c_R)^2 \frac{h_{\hat{K}_2}}{\rho_{\hat{K}_2}} \leq \sqrt{\frac{1 + c_\delta}{1 - c_\delta}} (1 + c_R)^2 \sigma_{\mathcal{K}} = \tilde{\sigma}_{\mathcal{K}} \end{aligned}$$

Obviously, the aspect ratio is uniformly bounded from above by a perturbed regularity parameter $\tilde{\sigma}_{\mathcal{K}}$.

Finally we address (iii) of Definition 1. Let \tilde{e} be an edge of \tilde{K}_2 with endpoints $\tilde{\mathbf{x}}_1$ and $\tilde{\mathbf{x}}_2$. Furthermore, let \hat{e} be the corresponding edge of \hat{K}_2 with endpoints $\hat{\mathbf{x}}_1$ and $\hat{\mathbf{x}}_2$. In the penultimate equation we estimated $h_{\tilde{K}_2}$ by a term times $h_{\hat{K}_2}$. Due to the regularity it is $h_{\tilde{K}_2} \leq c_{\mathcal{K}} |\hat{e}|$ and, as in the estimate of $\rho_{\hat{K}_2}$ above, we find that

$$\begin{aligned} |\hat{e}| &= |\hat{\mathbf{x}}_1 - \hat{\mathbf{x}}_2| = |F_{K_2} \circ F_{K_1}^{-1}(\tilde{\mathbf{x}}_1 - \tilde{\mathbf{x}}_2)| \\ &\leq \frac{\alpha_{K_2}}{\alpha_{K_1}} \max_{j=1,\dots,d} \left\{ (1 + \delta_j^{K_1, K_2})^{-1/2} \right\} \left(1 + \left(\frac{\lambda_{K_1,1}}{\lambda_{K_1,d}} \right)^{1/2} \|R^{K_1, K_2} - I\|_2 \right) |\tilde{e}|. \end{aligned}$$

Summarizing, we obtain

$$h_{\tilde{K}_2} \leq \sqrt{\frac{1 + c_\delta}{1 - c_\delta}} (1 + c_R)^2 c_{\mathcal{K}} |\tilde{e}| = \tilde{c}_{\mathcal{K}} |\tilde{e}|.$$

□

Remark 2. According to the previous proof, the perturbed regularity parameters are given by

$$\tilde{\sigma}_{\mathcal{K}} = \sqrt{\frac{1 + c_\delta}{1 - c_\delta}} (1 + c_R)^2 \sigma_{\mathcal{K}} \quad \text{and} \quad \tilde{c}_{\mathcal{K}} = \sqrt{\frac{1 + c_\delta}{1 - c_\delta}} (1 + c_R)^2 c_{\mathcal{K}}.$$

Proposition 1. *Let $K \in \mathcal{K}_h$ be a polytopal element of a regular anisotropic mesh \mathcal{K}_h and $E \in \mathcal{E}_h$ one of its edges ($d = 2$) or faces ($d = 3$). Then, the mapped patches $F_K(\omega_K)$ and $F_K(\omega_E)$ consist of regular polytopal elements.*

Proof. The mapped patches $F_K(\omega_i)$, $i \in I(K)$ consist of regular polytopal elements according to Lemma 2. Since ω_K and ω_E are given as union of the neighbourhoods ω_i , the statement of the proposition follows. □

Proposition 2. *Each node \mathbf{x}_i of a regular anisotropic mesh \mathcal{K}_h belongs to a uniformly bounded number of elements. Vice versa, each element $K \in \mathcal{K}_h$ has a uniformly bounded number of nodes on its boundary.*

Proof. Let ω_i be the neighbourhood of the node x_i . According to Lemma 2, the mapped neighbourhood $\tilde{\omega}_i$ consists of regular polytopal elements, which admit a shape-regular decomposition into simplices (triangles or tetrahedra). The mapped node $\tilde{\mathbf{x}}_i$ therefore belongs to a uniformly bounded number of simplices and thus to finitely many polytopal elements, cf. [26, 28]. Since $\tilde{\omega}_i$ is obtained by a linear transformation, we follow that \mathbf{x}_i belongs to a uniformly bounded number of anisotropic elements. With the same argument we see that \tilde{K} and thus K has a uniformly bounded number of nodes on its boundary. □

Remark 3. In the publication of Apel and Kunert (see e.g. [2, 18]), it is assumed that neighbouring triangles/tetrahedra behave similarly. More precisely, they assume:

- The number of tetrahedra containing a node \mathbf{x}_i is bounded uniformly.
- The dimension of adjacent tetrahedra must not change rapidly, i.e.

$$h_{i,T} \sim h_{i,T'} \quad \forall T, T' \text{ with } T \cap T' \neq \emptyset, \quad i = 1, 2, 3,$$

where $h_{1,T} \geq h_{2,T} \geq h_{3,T}$ are the heights of the tetrahedron T over its faces.

The first point is always fulfilled in our setting according to the previous proposition. The second point corresponds to our assumption that Λ_{K_1} and Λ_{K_2} differ moderately for neighbouring elements K_1 and K_2 , see Definition 2. The assumption on U_{K_1} and U_{K_2} in the definition ensure that the heights are aligned in the same directions, this is also hidden in the assumption of Apel and Kunert.

The regularity of the mapped patches has several consequences, which are exploited in later proofs.

Lemma 3. *Let $K_1, K_2 \in \mathcal{K}_h$ be polytopal elements of a regular anisotropic mesh \mathcal{K}_h , ω_i and ω_{K_1} be the neighbourhoods of the node \mathbf{x}_i and the element K_1 , respectively. Then, we have for the mapped patch $\tilde{\omega} \in \{F_{K_1}(\omega_i), F_{K_1}(\omega_{K_1})\}$ and the neighbouring elements $K_1, K_2 \subset \omega_i$, that*

$$h_{\tilde{\omega}} \leq c \quad \text{and} \quad \frac{|K_2|}{|K_1|} \leq c,$$

where the constants only depend on the regularity parameters of the mesh.

Proof. According to Lemma 2 and Proposition 1 the patch $\tilde{\omega}$ consists of regular polytopal elements. Obviously, it is $h_{\tilde{\omega}} \leq 2 \max\{h_{\tilde{K}} : \tilde{K} \subset \tilde{\omega}\}$. Let us assume without loss of generality that the maximum is reached for \tilde{K} which shares a common edge \tilde{e} with \tilde{K}_1 . Otherwise consider a sequence of polytopal elements in $\tilde{\omega}$, see [26]. Due to the regularity of the elements, it is

$$h_{\tilde{\omega}} \leq 2h_{\tilde{K}} \leq 2c_{\mathcal{K}}|\tilde{e}| \leq 2c_{\mathcal{K}}h_{\tilde{K}_1} \leq \frac{2c_{\mathcal{K}}\sigma_{\mathcal{K}}}{(\nu\pi)^{1/d}}$$

according to (4), since $\tilde{K}_1 = F_{K_1}(K_1) = \widehat{K}_1$.

In order to prove the second estimate, we observe that $|K_1| = |\widehat{K}_1|/|\det(A_{K_1})|$, see Lemma 1. The same variable transform yields $|K_2| = |\tilde{K}_2|/|\det(A_{K_1})|$, where $\tilde{K}_2 = F_{K_1}(K_2)$. Thus, we obtain

$$\frac{|K_2|}{|K_1|} = \frac{|\tilde{K}_2|}{|\widehat{K}_1|} = |\tilde{K}_2| \leq |\tilde{\omega}_i| \leq h_{\tilde{\omega}_i}^d \leq c.$$

□

3. ANISOTROPIC TRACE INEQUALITY AND BEST APPROXIMATION

In this section we introduce some tools which are needed in later proofs. Here, the mapping (2) is employed to transform a regular anisotropic element K onto its reference configuration \widehat{K} , which is regular in the sense of Definition 1.

Lemma 4 (anisotropic trace inequality). *Let $K \in \mathcal{K}_h$ be a polytopal element of a regular anisotropic mesh \mathcal{K}_h with edge ($d = 2$) or face ($d = 3$) $E \in \mathcal{E}_h$, $E \subset \partial K$. It holds*

$$\|v\|_{L_2(E)}^2 \leq c \frac{|E|}{|K|} \left(\|v\|_{L_2(K)}^2 + \|A_K^{-\top} \nabla v\|_{L_2(K)}^2 \right),$$

where the constant c only depends on the regularity parameters of the mesh.

Proof. In order to prove the estimate, we make use of the transformation (2) to the reference configuration \widehat{K} with $\widehat{v} = v \circ F_K^{-1}$, a trace inequality on \widehat{K} , see [4, 26, 28], as well as of (4), (5) and $h_{\widehat{K}}^{-d} \leq |\widehat{K}|^{-1} = 1$:

$$\begin{aligned} \|v\|_{L_2(E)}^2 &= \frac{|E|}{|\widehat{E}|} \|\widehat{v}\|_{L_2(\widehat{E})}^2 \\ &\leq c \frac{|E|}{|\widehat{E}|} \left(h_{\widehat{K}}^{-1} \|\widehat{v}\|_{L_2(\widehat{K})}^2 + h_{\widehat{K}} |\widehat{v}|_{H^1(\widehat{K})}^2 \right) \\ &\leq c |E| h_{\widehat{K}}^{-d} \left(\|\widehat{v}\|_{L_2(\widehat{K})}^2 + h_{\widehat{K}}^2 |\widehat{v}|_{H^1(\widehat{K})}^2 \right) \\ &\leq c |E| \left(\|\widehat{v}\|_{L_2(\widehat{K})}^2 + \|\widehat{\nabla} \widehat{v}\|_{L_2(\widehat{K})}^2 \right) \\ &= c \frac{|E|}{|K|} \left(\|v\|_{L_2(K)}^2 + \|A^{-\top} \nabla v\|_{L_2(K)}^2 \right). \end{aligned}$$

□

Remark 4. If we plug in the definition of $A = \alpha \Lambda_K^{-1/2} U_K^\top$, we have the anisotropic trace inequality

$$\|v\|_{L_2(E)}^2 \leq c \frac{|E|}{|K|} \left(\|v\|_{L_2(K)}^2 + \|\alpha^{-1} \Lambda_K^{1/2} U_K^\top \nabla v\|_{L_2(K)}^2 \right).$$

Obviously, the derivatives of v in the directions $\mathbf{u}_{K,j}$ are scaled by $\lambda_j^{1/2}$, $j = 1, \dots, d$. This seems to be appropriate for functions with anisotropic behaviour which are aligned with the mesh.

For later comparisons with other methods, we bound the term $|E|/|K|$ in case of $E \subset \partial K$. Let $\mathbf{z}_{\widehat{K}}$ be the midpoint of the circle/ball in Definition 1 of the regular reference configuration \widehat{K} . Obviously, it is $|K| \geq |P|$ for the d -dimensional pyramid with base side E and apex point $F_K^{-1}(\mathbf{z}_{\widehat{K}})$, since $P \subset K$ due to the linearity of F_K . Let $h_{P,E}$ be the hight of this pyramid, then it is $|P| = \frac{1}{3}|E|h_{P,E}$ and we obtain

$$(6) \quad \frac{|E|}{|K|} \leq c h_{P,E}^{-1}.$$

In the derivation of approximation estimates, the Poincaré constant plays a crucial role. For a domain $\omega \subset \mathbb{R}^d$, $d = 2, 3$, it is defined by

$$(7) \quad C_P(\omega) = \sup_{v \in H^1(\omega)} \frac{\|v - \Pi_\omega v\|_{L_2(\omega)}}{h_\omega |v|_{H^1(\omega)}} < \infty,$$

where h_ω is the diameter of ω and Π_ω denotes the L_2 -projection over ω into constants, i.e.

$$\Pi_\omega v = \frac{1}{|\omega|} \int_\omega v(\mathbf{x}) d\mathbf{x}.$$

Lemma 5. *Let \mathcal{K}_h be a regular anisotropic mesh, ω_i and ω_K be patches as described above, and $K \in \mathcal{K}_h$ with $K \subset \omega_i$. The Poincaré constants $C_P(\tilde{\omega}_i)$ and $C_P(\tilde{\omega}_K)$ for the mapped patches $\tilde{\omega}_i = F_K(\omega_i)$ and $\tilde{\omega}_K = F_K(\omega_K)$, respectively, can be bounded uniformly depending only on the regularity parameters of the mesh.*

Proof. According to Lemma 2 and Proposition 1, the patches $\tilde{\omega}_i$ and $\tilde{\omega}_K$ consist of regular polytopal elements, which admit a shape-regular auxiliary triangulation with a uniformly bounded number of simplices. Thus, we can proceed as in [4] in order to prove the existence of a constant C^{Int} such that for $v \in H^1(\tilde{\omega})$, $\tilde{\omega} \in \{\tilde{\omega}_i, \tilde{\omega}_K\}$ there exists a constant p such that

$$\|v - p\|_{L_2(\tilde{\omega})} + h_{\tilde{\omega}}|v|_{H^1(\tilde{\omega})} \leq C^{Int} h_{\tilde{\omega}}|v|_{H^1(\tilde{\omega})},$$

where C^{Int} only depends on the regularity of the triangulation and the number of simplices therein. Since $\|v - \Pi_{\tilde{\omega}}v\|_{L_2(\tilde{\omega})} \leq \|v - p\|_{L_2(\tilde{\omega})}$, the statement of the proposition follows. See also the results from [26, 28] for $d = 2$. \square

Next, we derive a best approximation result on patches of anisotropic elements.

Lemma 6. *Let \mathcal{K}_h be a regular anisotropic mesh with node \mathbf{x}_i and element $K \in \mathcal{K}_h$. Furthermore, let ω_i and ω_K be the neighbourhood of x_i and K , respectively, and we assume $K \subset \omega_i$. For $\omega \in \{\omega_i, \omega_K\}$ it holds*

$$\|v - \Pi_{\omega}v\|_{L_2(\omega)} \leq c \|A_K^{-\top} \nabla v\|_{L_2(\omega)},$$

and furthermore

$$\|v - \Pi_{\omega}v\|_{L_2(\omega)} \leq c \left(\sum_{K' \in \mathcal{K}_h: K' \subset \omega} \|A_{K'}^{-\top} \nabla v\|_{L_2(K')}^2 \right)^{1/2},$$

where the constant c only depends on the regularity parameters of the mesh.

Proof. We make use of the mapping (2) and indicate the objects on the mapped geometry with a tilde, e.g., $\tilde{\omega} = F_K(\omega)$. Furthermore, we exploited that the mapped L_2 -projection coincides with the L_2 -projection on the mapped patch, i.e. $\Pi_{\omega}v = \Pi_{\tilde{\omega}}\tilde{v}$. This yields together with Lemma 5

$$\begin{aligned} \|v - \Pi_{\omega}v\|_{L_2(\omega)} &= |K|^{1/2} \|\tilde{v} - \Pi_{\tilde{\omega}}\tilde{v}\|_{L_2(\tilde{\omega})} \\ &\leq ch_{\tilde{\omega}}|K|^{1/2} |\tilde{v}|_{H^1(\tilde{\omega})} \\ &= ch_{\tilde{\omega}}|K|^{1/2} \|\tilde{\nabla}\tilde{v}\|_{L_2(\tilde{\omega})} \\ &= ch_{\tilde{\omega}} \|A_K^{-\top} \nabla v\|_{L_2(\omega)}. \end{aligned}$$

The term $h_{\tilde{\omega}}$ is uniformly bounded according to Lemma 3, and thus the first estimate is proved.

In order to prove the second estimate, we employ the first one and write

$$\|v - \Pi_{\omega}v\|_{L_2(\omega)}^2 \leq c \|A_K^{-\top} \nabla v\|_{L_2(\omega)}^2 = c \sum_{K' \in \mathcal{K}_h: K' \subset \omega} \|A_{K'}^{-\top} \nabla v\|_{L_2(K')}^2.$$

Therefore, it remains to estimate $\|A_K^{-\top} \nabla v\|_{L_2(K')}$ by $\|A_{K'}^{-\top} \nabla v\|_{L_2(K')}$ for any $K' \subset \omega$. We make use of the mesh regularity, see Definition 2, and proceed similar as in the

proof of Lemma 2.

$$\begin{aligned}
\|A_K^{-\top} \nabla v\|_{L_2(K')} &= \frac{\alpha_{K'}}{\alpha_K} \|\alpha_{K'}^{-1} ((I + \Delta^{K',K}) \Lambda_{K'})^{1/2} (R^{K',K} U_{K'})^\top \nabla v\|_{L_2(K')} \\
&= \frac{\alpha_{K'}}{\alpha_K} \|\alpha_{K'}^{-1} (I + \Delta^{K',K})^{1/2} \Lambda_{K'}^{1/2} U_{K'}^\top (R^{K',K})^\top \nabla v\|_{L_2(K')} \\
&= \frac{\alpha_{K'}}{\alpha_K} \|\alpha_{K'}^{-1} (I + \Delta^{K',K})^{1/2} \Lambda_{K'}^{1/2} U_{K'}^\top (R^{K',K})^\top U_{K'} \Lambda_{K'}^{-1/2} \Lambda_{K'}^{1/2} U_{K'}^\top \nabla v\|_{L_2(K')} \\
&\leq \frac{\alpha_{K'}}{\alpha_K} \|(I + \Delta^{K',K})^{1/2} \Lambda_{K'}^{1/2} U_{K'}^\top (R^{K',K})^\top U_{K'} \Lambda_{K'}^{-1/2}\|_2 \|A_{K'}^{-\top} \nabla v\|_{L_2(K')},
\end{aligned}$$

where we substituted $A_K^{-\top} = \alpha_{K'}^{-1} \Lambda_{K'}^{1/2} U_{K'}^\top$. Finally, we have to bound the ratio $\alpha_{K'}/\alpha_K$ and the matrix norm. According to the choice (3) and Lemma 3, it is

$$\begin{aligned}
\left(\frac{\alpha_{K'}}{\alpha_K}\right)^2 &= \frac{|K| \sqrt{\prod_{j=1}^d \lambda_{K',j}}}{|K'| \sqrt{\prod_{j=1}^d \lambda_{K,j}}} = \frac{|K| \sqrt{\prod_{j=1}^d (1 + \delta_j^{K,K'})} \lambda_{K,j}}{|K'| \sqrt{\prod_{j=1}^d \lambda_{K,j}}} \\
&\leq (1 + c_\delta)^{d/2} \frac{|K|}{|K'|} \leq c,
\end{aligned}$$

and for the matrix norm, we have

$$\begin{aligned}
&\|(I + \Delta^{K',K})^{1/2} \Lambda_{K'}^{1/2} U_{K'}^\top (R^{K',K})^\top U_{K'} \Lambda_{K'}^{-1/2}\|_2 \\
&\leq \|(I + \Delta^{K',K})^{1/2}\|_2 \|\Lambda_{K'}^{1/2} U_{K'}^\top (R^{K',K} - I)^\top U_{K'} \Lambda_{K'}^{-1/2} + I\|_2 \\
&\leq \sqrt{1 + c_\delta} (1 + c_R),
\end{aligned}$$

which finishes the proof. \square

Remark 5. In the previous proof, we have seen in particular that for neighbouring elements $K, K' \subset \omega_K$, it is

$$\|A_K^{-\top} \nabla v\|_{L_2(K')} \leq c \|A_{K'}^{-\top} \nabla v\|_{L_2(K')}$$

with a constant depending only on the regularity of the mesh.

4. QUASI-INTERPOLATION OF NON-SMOOTH FUNCTIONS

In this section, we study quasi-interpolation operators on anisotropic polygonal and polyhedral meshes. Classical results on simplicial meshes with isotropic elements go back to Clément [8] and to Scott and Zhang [23]. Quasi-interpolation operators on anisotropic simplicial meshes can be found in [2, 18], for example. Clément-type interpolation operators on polygonal meshes have been studied in [26, 28].

Having the application to boundary value problems in mind, we split the boundary of the domain $\Omega \subset \mathbb{R}^d$, $d = 2, 3$ into a Dirichlet Γ_D and Neumann Γ_N part such that $\partial\Omega = \bar{\Gamma}_D \cup \bar{\Gamma}_N$. We consider the Sobolev space

$$H_D^1(\Omega) = \{v \in H^1(\Omega) : v = 0 \text{ on } \Gamma_D\}$$

of functions with vanishing trace on Γ_D and we allow $\Gamma_D = \partial\Omega$ and $\Gamma_D = \emptyset$. Let \mathcal{K}_h be a regular anisotropic mesh of Ω such that the edges and faces \mathcal{E}_h are compatible with the Dirichlet and Neumann boundary. Furthermore, let the nodes \mathbf{x}_i be numbered such that they lie inside of Ω for $i = 1, \dots, N_{\text{int}}$, on Γ_N for $i =$

$N_{\text{int}}+1, \dots, N_{\text{DoF}}$ and on $\overline{\Gamma}_D$ for $i = N_{\text{DoF}}+1, \dots, N$. If $\Gamma_N = \emptyset$, we set $N_{\text{DoF}} = N_{\text{int}}$. The objective of this section is to define a quasi-interpolation operator

$$\mathfrak{I} : H_D^1(\Omega) \rightarrow V_h \cap H_D^1(\Omega),$$

which fulfils anisotropic interpolation error estimates and which preserves the homogeneous Dirichlet data. The discrete space V_h is given as discussed in Sec. 2.1 with basis functions ψ_i . Let $v \in H_D^1(\Omega)$, as usual we define

$$(8) \quad \mathfrak{I}v(\mathbf{x}) = \sum_{i=1}^{N_*} (\Pi_{\sigma_i} v)(\mathbf{x}_i) \psi_i(\mathbf{x})$$

for $\mathbf{x} \in \Omega$, where $\Pi_{\sigma_i} : L_2(\sigma_i) \rightarrow \mathcal{P}^0(\sigma_i)$ is the L_2 -projection into the space of constants over σ_i . The Clément and Scott-Zhang interpolation operators differ in the choice of σ_i and N_* .

4.1. Clément-type interpolation. The Clément interpolation operator \mathfrak{I}_C is defined as usual by (8), where we choose $N_* = N_{\text{DoF}}$ and $\sigma_i = \omega_i$. Thus, it is given as a linear combination of the basis functions ψ_i associated to the nodes in the interior of Ω and the Neumann boundary Γ_N . The expansion coefficients are chosen as average over the neighbourhood of the corresponding nodes. For $v \in H_D^1(\Omega)$, it is $\mathfrak{I}_C v \in H_D^1(\Omega)$ by construction.

Recall, that $I(K)$ and $I(E)$ denote the sets of indices of nodes which belong to the element K and the edge/face E , respectively. Similarly, we denote by $I(\Gamma_D)$ the set of indices of the nodes which are located on the Dirichlet boundary Γ_D . The following interpolation error estimates hold involving the neighbourhoods ω_K and ω_E of elements and edges/faces.

Theorem 1. *Let \mathcal{K}_h be a regular anisotropic mesh with nodes \mathbf{x}_i as described above. Furthermore, let ω_i be the neighbourhood of \mathbf{x}_i and $K \in \mathcal{K}_h$. For $v \in H_D^1(\Omega)$, it is*

$$\|v - \mathfrak{I}_C v\|_{L_2(K)} \leq c \|A_K^{-\top} \nabla v\|_{L_2(\omega_K)},$$

and for an edge/face $E \in \mathcal{E}_h$ with $E \subset \partial K \setminus \Gamma_D$

$$\|v - \mathfrak{I}_C v\|_{L_2(E)} \leq c \frac{|E|^{1/2}}{|K|^{1/2}} \|A_K^{-\top} \nabla v\|_{L_2(\omega_E)},$$

where the constants c only depend on the regularity parameters of the mesh.

Proof. We can follow classical arguments as for isotropic meshes, cf. [25], and see the adaptation to polygonal meshes in [26]. The main ingredients are the observation that the basis functions ψ_i form a partition of unity, i.e. $\sum_{i \in I(K)} \psi_i = 1$ on \overline{K} , and that they fulfil $\|\psi_i\|_{L_\infty(\overline{K})} = 1$. Furthermore, anisotropic approximation estimates, see Lemma 6, the trace inequality in Lemma 4, Lemma 3 and Remark 5 are employed. We only sketch the proof of the second estimate.

The partition of unity property is used, which also holds on each edge/face E , i.e. $\sum_{i \in I(E)} \psi_i = 1$ on \overline{E} . We distinguish two cases, first let $I(E) \cap I(\Gamma_D) = \emptyset$. With

the help of Lemma 4 and Lemma 6, we obtain

$$\begin{aligned}
\|v - \mathfrak{I}_C v\|_{L_2(E)} &= \sum_{i \in I(E)} \|\psi_i(v - \Pi_{\omega_i} v)\|_{L_2(E)} \leq \sum_{i \in I(E)} \|v - \Pi_{\omega_i} v\|_{L_2(E)} \\
&\leq c \sum_{i \in I(E)} \frac{|E|^{1/2}}{|K|^{1/2}} \left(\|v - \Pi_{\omega_i} v\|_{L_2(K)}^2 + \|A_K^{-\top} \nabla v\|_{L_2(K)}^2 \right)^{1/2} \\
&\leq c \sum_{i \in I(E)} \frac{|E|^{1/2}}{|K|^{1/2}} \|A_K^{-\top} \nabla v\|_{L_2(\omega_i)}.
\end{aligned}$$

For the second case $I(E) \cap I(\Gamma_D) \neq \emptyset$, we find

$$(9) \quad \|v - \mathfrak{I}_C v\|_{L_2(E)} \leq \sum_{i \in I(E)} \|\psi_i(v - \Pi_{\omega_i} v)\|_{L_2(E)} + \sum_{i \in I(E) \cap I(\Gamma_D)} \|\psi_i \Pi_{\omega_i} v\|_{L_2(E)}.$$

The first sum has already been estimated, thus we consider the term in the second sum. For $i \in I(E) \cap I(\Gamma_D)$, i.e. $\mathbf{x}_i \in \bar{\Gamma}_D$, there is an element $K' \subset \omega_i$ and an edge/face $E' \subset \bar{K}' \cap \Gamma_D$ such that $\mathbf{x}_i \in \bar{E}'$. Since v vanishes on E' , Lemmata 4 and 6 as well as Remark 5 yield

$$|\Pi_{\omega_i} v| = |E'|^{-1/2} \|v - \Pi_{\omega_i} v\|_{L_2(E')} \leq c |K'|^{-1/2} \|A_K^{-\top} \nabla v\|_{L_2(\omega_i)}.$$

Because $|K'|/|K|$ is uniformly bounded according to Lemma 3, we obtain

$$\|\psi_i \Pi_{\omega_i} v\|_{L_2(E)} \leq |\Pi_{\omega_i} v| \|\psi_i\|_{L_\infty(E)} |E|^{1/2} \leq c \frac{|E|^{1/2}}{|K|^{1/2}} \|A_K^{-\top} \nabla v\|_{L_2(\omega_i)}.$$

Finally, since the number of nodes per element is uniformly bounded according to Proposition 2, this estimate as well as the one derived in the first case applied to (9) yield the second interpolation error estimate in the theorem. \square

Remark 6. In the case of an isotropic polytopal element K with edge/face E it is

$$\lambda_1 \approx \dots \approx \lambda_d \sim h_K^2, \quad \text{and thus} \quad \alpha_K \sim 1.$$

Therefore, we obtain from Theorem 1 with $A_K^{-\top} = \alpha_K^{-1} \Lambda_K^{1/2} U_K^\top$ that

$$\|v - \mathfrak{I}_C v\|_{L_2(K)} \leq ch_K \|U_K^\top \nabla v\|_{L_2(\omega_K)} = ch_K |v|_{H^1(\omega_K)},$$

and

$$\|v - \mathfrak{I}_C v\|_{L_2(E)} \leq c \frac{h_K |E|^{1/2}}{|K|^{1/2}} \|U_K^\top \nabla v\|_{L_2(\omega_E)} \leq ch_E^{1/2} |v|_{H^1(\omega_E)},$$

since $|E| \leq h_E^{d-1}$ as well as $|K| \geq ch_K^d$ and $h_K \leq ch_E$ in consequence of Definition 1. Obviously, we recover the classical interpolation error estimates for the Clément interpolation operator, cf., e.g., [25, 28].

In the following, we rewrite our results in order to compare them with the work of Formaggia and Perotto [12]. It is $A_K^{-\top} = \alpha_K^{-1} \Lambda_K^{1/2} U_K^\top$ with $U_K = (\mathbf{u}_{K,1}, \dots, \mathbf{u}_{K,d})$. Thus, we observe

$$\|A_K^{-\top} \nabla v\|_{L_2(\omega_K)}^2 = \alpha_K^{-2} \sum_{j=1}^d \lambda_{K,j} \|\mathbf{u}_{K,j} \cdot \nabla v\|_{L_2(\omega_K)}^2,$$

and since $\mathbf{u}_{K,j} \cdot \nabla v \in \mathbb{R}$, we obtain

$$\|\mathbf{u}_{K,j} \cdot \nabla v\|_{L_2(\omega_K)}^2 = \sum_{K' \subset \omega_K} \int_{K'} \mathbf{u}_{K,j}^\top \nabla v (\nabla v)^\top \mathbf{u}_{K,j} \, d\mathbf{x} = \mathbf{u}_{K,j}^\top G_K(v) \mathbf{u}_{K,j}$$

with

$$G_K(v) = \sum_{K' \subset \omega_K} \left(\int_{K'} \frac{\partial v}{\partial x_i} \frac{\partial v}{\partial x_j} \, d\mathbf{x} \right)_{i,j=1}^d \in \mathbb{R}^{d \times d}, \quad \mathbf{x} = (x_1, \dots, x_d)^\top.$$

Therefore, we can deduce from Theorem 1 an equivalent formulation.

Proposition 3. *Let $K \in \mathcal{K}_h$ be a polytopal element of a regular anisotropic mesh. The Clément interpolation operator fulfils for $v \in H^1(\Omega)$ the interpolation error estimate*

$$\|v - \mathfrak{I}_C v\|_{L_2(K)} \leq c \alpha_K^{-1} \left(\sum_{j=1}^d \lambda_{K,j} \mathbf{u}_{K,j}^\top G_K(v) \mathbf{u}_{K,j} \right)^{1/2},$$

and

$$\|v - \mathfrak{I}_C v\|_{L_2(E)} \leq c \alpha_K^{-1} \frac{|E|^{1/2}}{|K|^{1/2}} \left(\sum_{j=1}^d \lambda_{K,j} \mathbf{u}_{K,j}^\top G_K(v) \mathbf{u}_{K,j} \right)^{1/2},$$

where the constant c only depends on the regularity parameters of the mesh.

Now we are ready to compare the interpolation error estimates with the ones derived by Formaggia and Perotto. These authors considered the case of anisotropic triangular meshes, i.e. $d = 2$. The inequalities in Proposition 3 correspond to the derived estimates (2.12) and (2.15) in [12] but they are valid on much more general meshes. When comparing these estimates to the results of Formaggia and Perotto, one has to take care on the powers of the lambdas. The triangular elements in their works are scaled with $\lambda_{i,K}$, $i = 1, 2$ in the characteristic directions whereas the scaling in this paper is $\lambda_{K,i}^{1/2}$, $i = 1, 2$.

Obviously, the first inequality of the previous proposition corresponds to the derived estimate (2.12) in [12] up to the scaling factor α_K^{-1} . However, for convex elements the assumption

$$\alpha_K \sim 1, \quad \text{i.e.,} \quad |K| \sim \sqrt{\lambda_{K,1} \lambda_{K,2}},$$

seems to be convenient, since this means that the area of the element $|K|$ is proportional to the area of the inscribed ellipse $\pi \sqrt{\lambda_{K,1}} \sqrt{\lambda_{K,2}}$, which is given by the scaled characteristic directions of the element.

In order to recognize the relation of the second inequality under these assumptions, we estimate the term $|E|/|K|$ by (6) and by applying $h_{P,E} \geq \lambda_{K,2}^{1/2}$. This yields

$$\|v - \mathfrak{I}_C v\|_{L_2(E)} \leq c \left(\frac{1}{\lambda_{K,2}^{1/2}} \right)^{1/2} \left(\lambda_{K,1} \mathbf{u}_{K,1}^\top G_K(v) \mathbf{u}_{K,1} + \lambda_{K,2} \mathbf{u}_{K,2}^\top G_K(v) \mathbf{u}_{K,2} \right)^{1/2},$$

and shows the correspondence to [12], since h_K and $\lambda_{1,K}$ are proportional in the referred work.

4.2. Scott-Zhang-type interpolation. The Scott-Zhang interpolation operator $\mathfrak{I}_{SZ} : H^1(\Omega) \rightarrow V_h$ is defined as usual by (8), where we choose $N_* = N$ and $\sigma_i = E$, where $E \in \mathcal{E}_h$ is an edge ($d = 2$) or face ($d = 3$) with $\mathbf{x}_i \in \overline{E}$ and

$$E \subset \Gamma_D \text{ if } \mathbf{x}_i \in \overline{\Gamma}_D \quad \text{and} \quad E \subset \Omega \cup \Gamma_N \text{ if } \mathbf{x}_i \in \Omega \cup \Gamma_N.$$

Thus, the interpolation is given as a linear combination of all basis functions ψ_i . The expansion coefficients are chosen as average over edges and faces. For $v \in H_D^1(\Omega)$, it is $\mathfrak{I}_C v \in H_D^1(\Omega)$ by construction such that homogeneous Dirichlet data is preserved. We have the following local stability result, which can be utilized to derive interpolation error estimates.

Lemma 7. *Let $K \in \mathcal{K}_h$ be a polytopal element of a regular anisotropic mesh. The Scott-Zhang interpolation operator fulfils for $v \in H^1(\Omega)$ the local stability*

$$\|\mathfrak{I}_{SZ} v\|_{L_2(K)} \leq c \left(\|v\|_{L_2(\omega_K)} + \|A_K^{-\top} \nabla v\|_{L_2(\omega_K)} \right),$$

where the constant c only depends on the regularity parameters of the mesh.

Proof. Due to the stability of the L_2 -projection Π_{σ_i} we have $\|\Pi_{\sigma_i} v\|_{L_2(\sigma_i)} \leq \|v\|_{L_2(\sigma_i)}$. Furthermore, there exists $K_i \in \mathcal{K}_h$ with $\sigma_i \subset \partial K_i$ such that $K_i \subset \omega_K$. Therefore, we obtain with the anisotropic trace inequality, see Lemma 4,

$$\begin{aligned} |\Pi_{\sigma_i} v| &= |\sigma_i|^{-1/2} \|\Pi_{\sigma_i} v\|_{L_2(\sigma_i)} \\ &\leq c |K_i|^{-1/2} \left(\|v\|_{L_2(K_i)}^2 + \|\alpha_{K_i}^{-1} \Lambda_{K_i}^{1/2} U_{K_i}^\top \nabla v\|_{L_2(K_i)}^2 \right)^{1/2}, \end{aligned}$$

since $\sigma_i = E \in \mathcal{E}_h$. Utilizing this estimate and $\|\psi_i\|_{L_\infty(K)} = 1$ yields

$$\begin{aligned} \|\mathfrak{I}_{SZ} v\|_{L_2(K)} &\leq \sum_{i \in I(K)} \|(\Pi_{\sigma_i} v)(\mathbf{x}_i) \psi_i\|_{L_2(K)} \\ &\leq \sum_{i \in I(K)} |(\Pi_{\sigma_i} v)| \|\psi_i\|_{L_\infty(K)} |K|^{1/2} \\ &\leq c \sum_{i \in I(K)} \left(\|v\|_{L_2(K_i)}^2 + \|A_{K_i}^{-\top} \nabla v\|_{L_2(K_i)}^2 \right)^{1/2}, \end{aligned}$$

where we have used $|K|/|K_i| \leq c$ according to Lemma 3. Applying the Cauchy-Schwarz inequality, Remark 5 and exploiting that the number of nodes per element is uniformly bounded, see Proposition 2, finishes the proof. \square

Theorem 2. *Let $K \in \mathcal{K}_h$ be a polytopal element of a regular anisotropic mesh. The Scott-Zhang interpolation operator fulfils for $v \in H^1(\Omega)$ the interpolation error estimate*

$$\|v - \mathfrak{I}_{SZ} v\|_{L_2(K)} \leq \|A_K^{-\top} \nabla v\|_{L_2(\omega_K)},$$

where the constant c only depends on the regularity parameters of the mesh.

Proof. For $p = \Pi_{\omega_K} v \in \mathbb{R}$ it is obviously $p = \mathfrak{I}_{SZ} p$ and $\nabla p = 0$. The estimate in the theorem follows by Lemma 7 and the application of Lemma 6, since

$$\begin{aligned} \|v - \mathfrak{I}_{SZ} v\|_{L_2(K)} &\leq \|v - p\|_{L_2(K)} + \|\mathfrak{I}_{SZ}(v - p)\|_{L_2(K)} \\ &\leq c \left(\|v - p\|_{L_2(\omega_K)} + \|A_K^{-\top} \nabla v\|_{L_2(\omega_K)} \right) \\ &\leq c \|A_K^{-\top} \nabla v\|_{L_2(\omega_K)}. \end{aligned}$$

\square

5. POINTWISE INTERPOLATION OF SMOOTH FUNCTIONS

In the previous section, we considered quasi-interpolation of functions in $H^1(\Omega)$. However, we may also address classical interpolation employing point evaluations in the case that the function to be interpolated is sufficiently regular. This is possible for functions in $H^2(\Omega)$. In the following, we consider the pointwise interpolation of lowest order

$$(10) \quad \mathfrak{I}_{\text{pw}}v(\mathbf{x}) = \sum_{i=1}^N v(\mathbf{x}_i) \psi_i(\mathbf{x})$$

for $v \in H^2(\Omega)$ on anisotropic meshes. For the analysis it is sufficient to study the restriction of $\mathfrak{I}_{\text{pw}} : H^2(\Omega) \rightarrow V_h$ onto a single element $K \in \mathcal{K}_h$ and we denote this restriction by the same symbol

$$\mathfrak{I}_{\text{pw}} : H^2(K) \rightarrow V_h|_K.$$

Furthermore, we make use of the mapping to and from the reference configuration, cf. (2). As earlier, we mark the operators and functions defined over the reference configuration by a hat, as, for instance, $\hat{v} = v \circ F_K^{-1} : \hat{K} \rightarrow K$. We already used $\nabla v = \alpha_K U_K \Lambda_K^{-1/2} \hat{\nabla} \hat{v}$, and by employing some calculus we find

$$(11) \quad \hat{H}(\hat{v}) = \alpha_K^{-2} \Lambda_K^{1/2} U_K^\top H(v) U_K \Lambda_K^{1/2},$$

where $H(v)$ denotes the Hessian matrix of $v \in H^2(\Omega)$ and $\hat{H}(\hat{v})$ the corresponding Hessian on the reference configuration.

Lemma 8. *Let $K \in \mathcal{K}_h$ be a polytopal element of a regular anisotropic mesh \mathcal{K}_h . For $v \in H^1(K)$, it is*

$$\sqrt{\frac{\prod_{j=2}^d \lambda_{K,j}}{\lambda_{K,1}}} |\hat{v}|_{H^1(\hat{K})}^2 \leq |v|_{H^1(K)}^2 \leq \sqrt{\frac{\prod_{j=1}^{d-1} \lambda_{K,j}}{\lambda_{K,d}}} |\hat{v}|_{H^1(\hat{K})}^2.$$

Proof. Applying the transformation to the reference configuration yields

$$\begin{aligned} |v|_{H^1(K)}^2 &= \|\nabla v\|_{L_2(K)}^2 = |K| \|\alpha_K U_K \Lambda_K^{-1/2} \hat{\nabla} \hat{v}\|_{L_2(\hat{K})}^2 \\ &= |K| \alpha_K^2 \|\Lambda_K^{-1/2} \hat{\nabla} \hat{v}\|_{L_2(\hat{K})}^2 = |K| \alpha_K^2 \sum_{j=1}^d \lambda_{K,j}^{-1} \left\| \frac{\partial \hat{v}}{\partial \hat{x}_j} \right\|_{L_2(\hat{K})}^2. \end{aligned}$$

Since $\lambda_{K,1} \geq \dots \geq \lambda_{K,d}$, we obtain

$$\frac{|K| \alpha_K^2}{\lambda_{K,1}} |\hat{v}|_{H^1(\hat{K})}^2 \leq |v|_{H^1(K)}^2 \leq \frac{|K| \alpha_K^2}{\lambda_{K,d}} |\hat{v}|_{H^1(\hat{K})}^2.$$

Due to the choice (3) for α_K , it is $|K| \alpha_K^2 = \sqrt{\prod_{j=1}^d \lambda_{K,j}}$, that completes the proof. \square

In order to derive interpolation error estimates, we make use of interpolation results on isotropic polytopal elements which are regular in the sense of Definition 1, see, e.g., [27] or related works on VEM and generalized barycentric coordinates. First, we recognize the relation between the interpolation $\mathfrak{I}_{\text{pw}}v$ transferred to the

reference configuration \widehat{K} and the interpolation $\widehat{\mathfrak{J}}_{\text{pw}}\widehat{v}$ defined directly on \widehat{K} . Namely, it is

$$(12) \quad \widehat{\mathfrak{J}}_{\text{pw}}v = \widehat{\mathfrak{J}}_{\text{pw}}\widehat{v},$$

since only function evaluations in the nodes are involved. For the operator $\widehat{\mathfrak{J}}_{\text{pw}}$, we can apply known results. We use the convention that $H^0(K) = L_2(K)$.

Theorem 3. *Let $K \in \mathcal{K}_h$ be a polytopal element of a regular anisotropic mesh \mathcal{K}_h . For $v \in H^2(\Omega)$, it is*

$$|v - \mathfrak{J}_{\text{pw}}v|_{H^\ell(K)}^2 \leq c\alpha_K^{-4} S_\ell(K) \sum_{i,j=1}^d \lambda_{K,i} \lambda_{K,j} L_K(\mathbf{u}_{K,i}, \mathbf{u}_{K,j}; v)$$

with

$$S_\ell(K) = \begin{cases} 1, & \text{for } \ell = 0, \\ \frac{1}{|K|} \sqrt{\frac{\prod_{j=1}^{d-1} \lambda_{K,j}}{\lambda_{K,d}}}, & \text{for } \ell = 1, \end{cases}$$

where

$$L_K(\mathbf{u}_{K,i}, \mathbf{u}_{K,j}; v) = \int_K (\mathbf{u}_{K,i}^\top H(v) \mathbf{u}_{K,j})^2 d\mathbf{x} \quad \text{for } i, j = 1, \dots, d.$$

Proof. Property (12) together with the scaling to the reference configuration and Lemma 8 as well as (4) yield

$$\begin{aligned} |v - \mathfrak{J}_{\text{pw}}v|_{H^0(K)}^2 &\leq |K| S_\ell(K) \|\widehat{v} - \widehat{\mathfrak{J}}_{\text{pw}}\widehat{v}\|_{L_2(\widehat{K})}^2 \\ &\leq ch_{\widehat{K}}^{2(2-\ell)} |K| S_\ell(K) |\widehat{v}|_{H^2(\widehat{K})}^2 \\ &\leq c|K| S_\ell(K) |\widehat{v}|_{H^2(\widehat{K})}^2, \end{aligned}$$

where known interpolation estimates have been applied on the regular isotropic element \widehat{K} , see, e.g., [21, 27]. Next, we transform the H^2 -semi-norm back to the element K . Employing the mapping and the relation (11) gives

$$\begin{aligned} |\widehat{v}|_{H^2(\widehat{K})}^2 &= \int_{\widehat{K}} \|\widehat{H}(\widehat{v})\|_F^2 d\widehat{\mathbf{x}} \\ &= \frac{\alpha_K^{-4}}{|K|} \int_K \|\Lambda_K^{1/2} U_K^\top H(v) U_K \Lambda_K^{1/2}\|_F^2 d\mathbf{x}, \end{aligned}$$

where $\|\cdot\|_F$ denotes the Frobenius norm of a matrix. A small exercise yields

$$\|\Lambda_K^{1/2} U_K^\top H(v) U_K \Lambda_K^{1/2}\|_F^2 = \sum_{i,j=1}^d \lambda_{K,i} \lambda_{K,j} (\mathbf{u}_{K,i}^\top H(v) \mathbf{u}_{K,j})^2,$$

and consequently

$$|\widehat{v}|_{H^2(\widehat{K})}^2 = \frac{\alpha_K^{-4}}{|K|} \sum_{i,j}^d \lambda_{K,i} \lambda_{K,j} L_K(\mathbf{u}_{K,i}, \mathbf{u}_{K,j}; v).$$

Combining the derived results yields the desired estimates. \square

For the comparison with the work of Formaggia and Perotto we remember that their lambdas behave like $\lambda_{i,K} \sim \sqrt{\lambda_{K,i}}$, $i = 1, 2$. Employing the assumption $\alpha_K \sim 1$ raised in the comparison of Section 4.1, we find

$$\frac{\sqrt{\lambda_{K,1}/\lambda_{K,2}}}{|K|} \sim \frac{1}{\lambda_{K,2}}.$$

Therefore, we recognize that the estimates in Theorem 3 match the results of Lemma 2 in [12], but on much more general meshes.

6. NUMERICAL ASSESSMENT: ANISOTROPIC POLYTOPAL MESHES

In the introduction we already mentioned that polygonal and polyhedral meshes are much more flexible in meshing than classical finite element shapes. This is in particular true for the generation of anisotropic meshes. In this section we give a first numerical assessment on polytopal anisotropic mesh refinement. We propose a bisection approach that does not rely on any initially prescribed direction and which is applicable in two- and three-dimensions. Classical bisection approaches for triangular and tetrahedral meshes do not share this versatility and they have to be combined with additional strategies like edge swapping, node removal and local node movement, see [22].

Starting from the local interpolation error estimate in Theorem 1, we obtain the global version

$$\|v - \mathfrak{I}_C v\|_{L_2(\Omega)} \leq c \left(\sum_{K \in \mathcal{K}_h} \|A_K^{-\top} \nabla v\|_{L_2(K)}^2 \right)^{1/2}$$

by exploiting Remark 5 and Proposition 2. As in the derivation of Proposition 3, we easily see that

$$\eta = \sqrt{\sum_{K \in \mathcal{K}_h} \eta_K} \quad \text{with} \quad \eta_K = \alpha_K^{-2} \sum_{j=1}^d \lambda_{K,j} \mathbf{u}_{K,j}^\top G_K^*(v) \mathbf{u}_{K,j}$$

and

$$G_K^*(v) = \left(\int_K \frac{\partial v}{\partial x_i} \frac{\partial v}{\partial x_j} d\mathbf{x} \right)_{i,j=1}^d \in \mathbb{R}^{d \times d}, \quad \mathbf{x} = (x_1, \dots, x_d)^\top.$$

is a good error measure and the local values η_K may serve as error indicators over the polytopal elements. This estimate also remains meaningful on isotropic polytopal meshes, cf. Remark 6. In the case that $v \in H^1(\Omega)$ and its derivatives are known, we can thus apply the following adaptive mesh refinement algorithm:

- (i) Let \mathcal{K}_0 be a given initial mesh and $\ell = 0$.
- (ii) Compute the error indicators η_K and η with the knowledge of the exact function v and its derivatives.
- (iii) Mark all elements K for refinement which fulfil $\eta_K > 0.9\eta^2/|\mathcal{K}_\ell|$, where $|\mathcal{K}_\ell|$ is the number of elements in the current mesh.
- (iv) Refine the marked elements as described below in order to obtain a refined mesh $\mathcal{K}_{\ell+1}$.
- (v) Go to (ii).

In step (iii), we have chosen a equidistribution strategy which marks all elements for refinement whose error indicator is larger than the mean value. The factor 0.9 has been chosen for stabilizing reasons in the computations when the error is almost

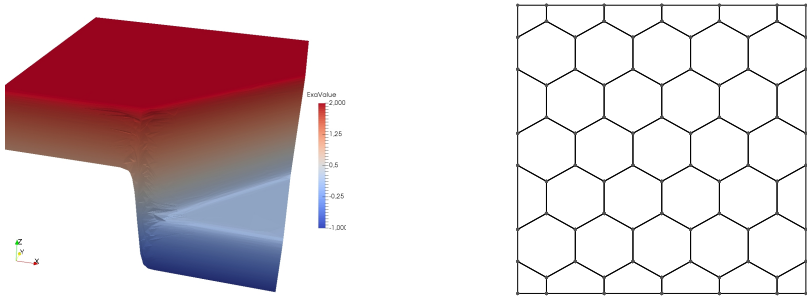


FIGURE 4. Visualization of function with anisotropic behaviour (left) and initial mesh (right)

uniformly distributed. For the refinement in step (iv), we have a closer look at the first term in the sum of η_K , which reads

$$\lambda_{K,1} \frac{\mathbf{u}_{K,1}^\top G_K^*(v) \mathbf{u}_{K,1}}{\mathbf{u}_{K,1}^\top \mathbf{u}_{K,1}},$$

because of $|\mathbf{u}_{K,1}| = 1$. Since $\lambda_{K,1} \gg \lambda_{K,d}$ for anisotropic elements, the refinement process should try to minimize the quotient such that the whole term does not dominate the error over K . Obviously, we are dealing here with the Rayleigh quotient, which is minimal if $\mathbf{u}_{K,1}$ is the eigenvector to the smallest eigenvalue of $G_K^*(v)$. As consequence, the longest stretching of the polytopal element K should be aligned with the direction of this eigenvector. In order to achieve the correct alignment for the next refined mesh, we may bisect the polytopal element orthogonal to the eigenvector which belongs to the largest eigenvalue of $G_K^*(v)$. Thus, we propose the following refinement strategies:

ISOTROPIC: The elements are bisected as introduced in [26], i.e., they are split orthogonal to the eigenvector corresponding to the largest eigenvalue of $M_{\text{Cov}}(K)$.

ANISOTROPIC: In order to respect the anisotropic nature of v , we split the elements orthogonal to the eigenvector corresponding to the largest eigenvalue of $G_K^*(u)$.

For the numerical experiments we consider $\Omega = (0, 1)^2$ and the function

$$(13) \quad v(x_1, x_2) = \tanh(60x_2) - \tanh(60(x_1 - x_2) - 30),$$

taken from [16], which has two sharp layers: one along the x_1 -axis and one along the line given by $x_2 = x_1 - 0.5$. The function as well as the initial mesh is depicted in Fig. 4.

6.1. Test: mesh refinement. In the first test we generate several sequences of polygonal meshes starting from an initial grid, see Fig. 4 right. These meshes contain naturally hanging nodes and their element shapes are quite general. First, the initial mesh is refined uniformly, i.e. all elements of the discretization are bisected in each refinement step. Here, the ISOTROPIC strategy is performed for the bisection. The mesh after 6 refinements as well as a zoom-in is depicted in Fig. 5. The uniform refinement clearly generates a lot of elements in regions where the function (13) is flat and where only a few elements would be sufficient for the approximation.

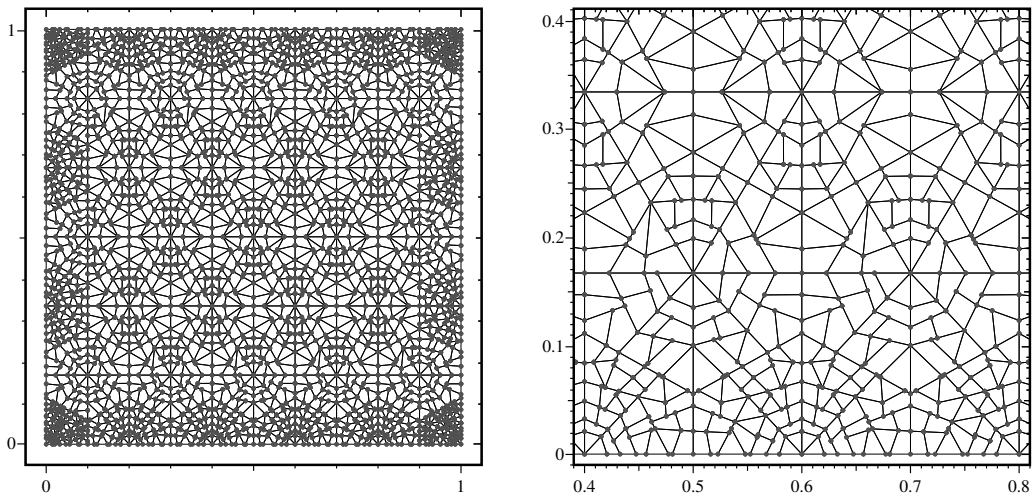


FIGURE 5. Mesh after 6 uniform refinement steps using the ISOTROPIC strategy and zoom-in

Next, we perform the adaptive refinement algorithm as described above for the different bisection strategies. The generated meshes after 6 refinement steps are visualized in the Figs. 6 and 7 together with a zoom-in of the region where the two layers of the function (13) meet. Both strategies detect the layers and adapt the refinement to the underlying function. The adaptive strategies clearly outperform the uniform refinement with respect to the number of nodes which are needed to resolve the layers. Whereas the ISOTROPIC strategy in Fig. 6 keeps the aspect ratio of the polygonal elements bounded, the ANISOTROPIC bisection produces highly anisotropic elements, see Fig. 7. These anisotropic elements coincide with the layers of the function very well.

Finally, we compare the error measure η for the different strategies. This value is given with respect to the number of degrees of freedom, which coincides with the number of nodes, in a double logarithmic plot in Fig. 8. The error measure decreases most rapidly for the ANISOTROPIC strategy and consequently these meshes are most appropriate for the approximation of the function (13). The slope corresponds to quadratic convergence in finite element analysis.

6.2. Test: mesh properties. We analyse the meshes more carefully. For this purpose we pick the 13th mesh of the sequence generated with the ISOTROPIC and the ANISOTROPIC refinement strategy. In Sec. 2.2, we have introduced the ratio $\lambda_{K,1}/\lambda_{K,2}$ for the characterisation of the anisotropy of an element. In Fig. 9, we give this ratio with respect to the element ids for the two chosen meshes. For the ISOTROPIC refined mesh the ratio is clearly bounded by 10 and therefore the mesh consists of isotropic elements according to our characterisation. In the ANISOTROPIC refined mesh, however, the ratio varies in a large interval. The mesh consists of several isotropic elements, but there are mainly anisotropic polygons. The ratio of the most anisotropic elements exceeds 10^5 in this example.

Next we address the scaling parameter α_K in these meshes. In the comparison of the derived estimates with those of Formaggia and Perotto [12], it has been assumed that $\alpha_K \sim 1$. In Fig. 10, we present a histogram for the distribution of α_K in the two selected meshes. As expected the values stay bounded for the ISOTROPIC

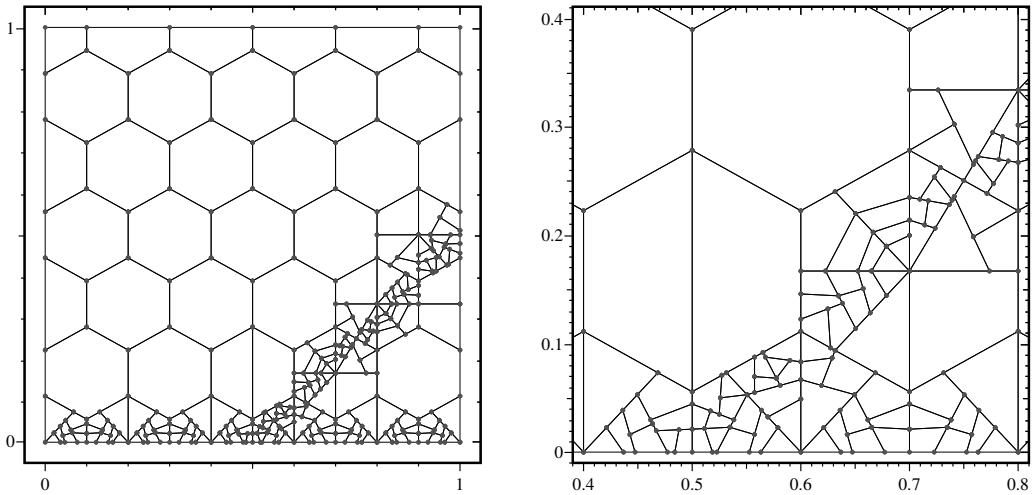


FIGURE 6. Mesh after 6 adaptive refinement steps for the ISOTROPIC strategy and zoom-in

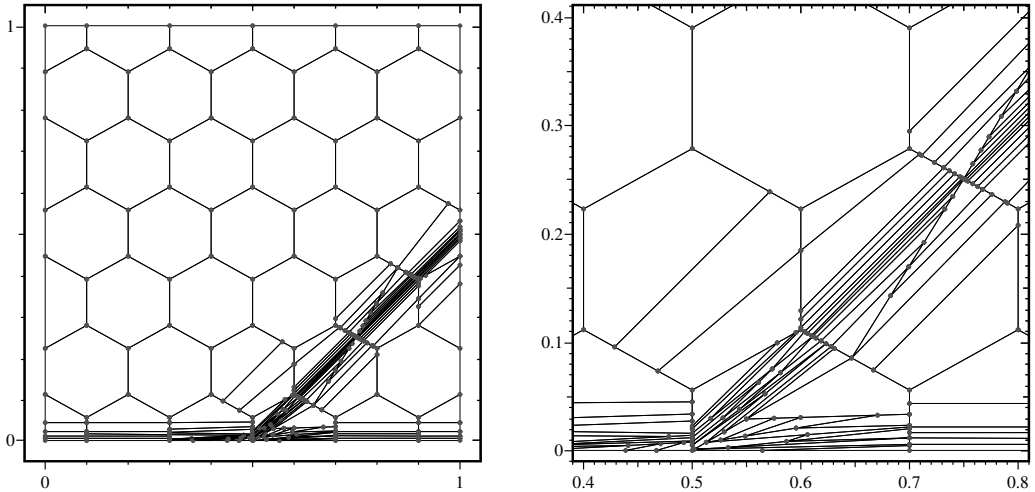


FIGURE 7. Mesh after 6 adaptive refinement steps for the ANISOTROPIC strategy and zoom-in

refined mesh. Furthermore, α_K stays in the same range for the ANISOTROPIC refinement. In our example, all values lie in the interval $(0.28, 0.32)$ although we are dealing with elements of quite different aspect ratios, cf. Fig. 9.

6.3. Test: interpolation error. In the last test we apply the pointwise interpolation operator (10) to the function (13) over the meshes generated in Sec. 6.1 and study numerically the convergence. The computations are done with a BEM-based FEM implementation written in C. For more details we refer the interested reader to [20]. Here, the implicitly defined basis functions ψ_i are treated locally by means of boundary element methods (BEM). The implementation uses the coarsest possible BEM discretization and it is not yet adapted to handle anisotropic elements. Due to the existence of a representation formula, it is possible to evaluate ψ_i inside the elements and thus to approximate, e.g., the L_2 -norm with the help of numerical quadrature over polygonal elements.

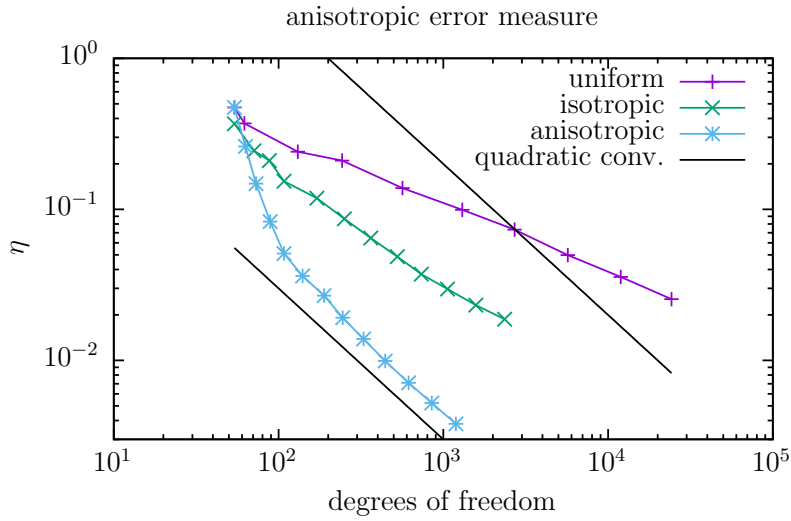


FIGURE 8. Convergence graph of the anisotropic error measure η with respect to the number of degrees of freedom for the different refinement strategies

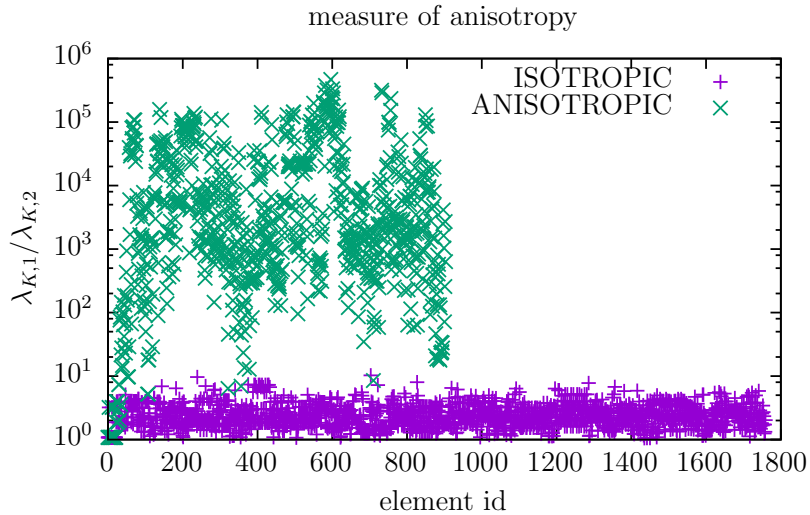


FIGURE 9. Quotient $\lambda_{K,1}/\lambda_{K,2}$ for all elements in the 13th mesh of the sequence with ISOTROPIC and ANISOTROPIC refinement

The convergence of the interpolation is studied numerically for the different sequences of meshes. We consider the interpolation error in the L_2 -norm. In Fig. 11, we give $\|v - \mathfrak{I}_{pw}v\|_{L_2(\Omega)}$ with respect to the number of degrees of freedom in a double logarithmic plot. Since $v \in H^2(\Omega)$ in this experiment, we expect quadratic convergence with respect to the mesh size on the sequence of uniform refined meshes. This convergence rate corresponds to a slope of one in the double logarithmic plot in two-dimensions. In Fig. 11, we observe that the uniform refinement reaches indeed quadratic convergence after a pre-asymptotic regime. The optimal rate of convergence is achieved as soon as the layers are resolved in the mesh. On the adaptive generated meshes, however, the interpolation error converges with optimal rates

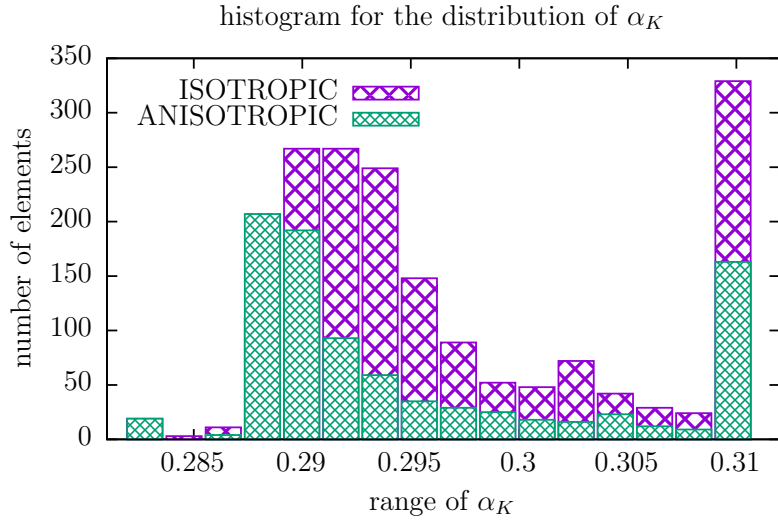


FIGURE 10. Histogram for the distribution of α_K for the 13th mesh in the sequence with ISOTROPIC and ANISOTROPIC refinement

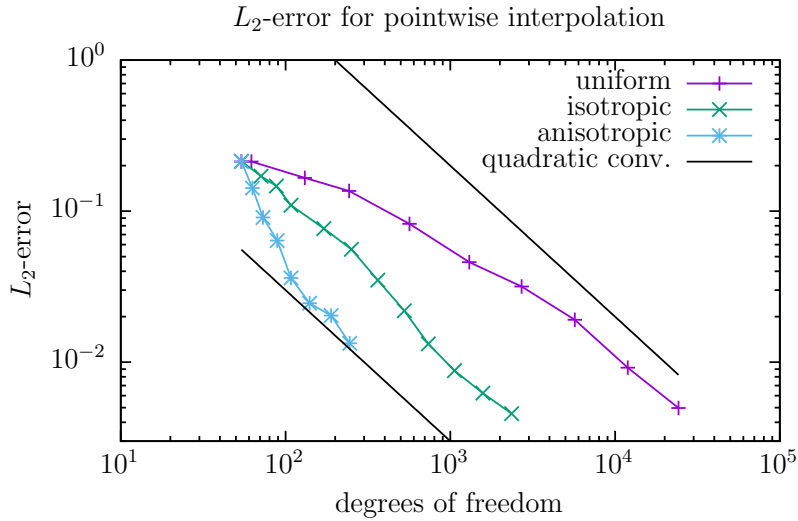


FIGURE 11. Convergence graph of the L_2 -error with respect to the number of degrees of freedom for the different refinement strategies

from the beginning. We can even recognize in Fig. 11 that the ANISOTROPIC refined meshes outperforms the others. The layers are captured within a few refinement steps and therefore the error reduces faster than for the ISOTROPIC refined meshes before it reaches the optimal convergence rate.

Let us compare the seventh meshes in the sequences which are obtained after six refinements and which are visualized in Figs. 5–7. For the uniform refined mesh we have 2709 nodes and it is $\|v - \mathcal{I}_{\text{pw}}v\|_{L_2(\Omega)} \approx 3.17 \cdot 10^{-2}$. The adaptive refined mesh using ISOTROPIC bisection contains only 363 nodes but yields a comparable error $\|v - \mathcal{I}_{\text{pw}}v\|_{L_2(\Omega)} \approx 3.49 \cdot 10^{-2}$. The most accurate approximation is achieved on the ANISOTROPIC refined mesh with $\|v - \mathcal{I}_{\text{pw}}v\|_{L_2(\Omega)} \approx 2.04 \cdot 10^{-2}$ and only 189 nodes. A comparable interpolation error to the other refinement strategies is

obtained on the fifth mesh of the sequence of ANISOTROPIC refined meshes. This mesh consists of 108 nodes only.

7. CONCLUSION

As seen in the previous section, polygonal elements allow for highly anisotropic meshes which are aligned to layers of the approximated function. Since hanging nodes are naturally included in the discretization, the refinements in the mesh are kept very local. These two properties result in the fact that approximations on anisotropic polytopal meshes are as accurate as on uniform and adaptive isotropic meshes but involving much less degrees of freedom. In consequence, the computational cost is reduced and therefore the efficiency increases.

The results for the derived interpolation and quasi-interpolation operators and their a priori error estimates are in accordance with previous works on classical element shapes. However, the new findings are applicable on much more general anisotropic polytopal meshes. In future projects we aim to apply our results for adaptive finite element strategies involving a posteriori error estimates on polytopal meshes for boundary value problems with highly anisotropic solutions.

ACKNOWLEDGEMENT

The author would like to thank Paola Antonietti and Marco Verani for their valuable comments during a research stay at the Laboratory for Modeling and Scientific Computing MOX, Dipartimento di Matematica, Politecnico di Milano, Italy.

REFERENCES

- [1] R. A. Adams. *Sobolev Spaces*. Academic Press, 1975.
- [2] T. Apel. *Anisotropic finite elements: local estimates and applications*. Advances in Numerical Mathematics. B. G. Teubner, Stuttgart, 1999.
- [3] L. Beirão da Veiga, F. Brezzi, A. Cangiani, G. Manzini, L. D. Marini, and A. Russo. Basic principles of virtual element methods. *Math. Models Methods Appl. Sci.*, 23(01):199–214, 2013.
- [4] L. Beirão da Veiga, K. Lipnikov, and G. Manzini. *The mimetic finite difference method for elliptic problems*, volume 11 of *MS&A. Modeling, Simulation and Applications*. Springer, Cham, 2014.
- [5] L. Beirão da Veiga and G. Manzini. Residual *a posteriori* error estimation for the virtual element method for elliptic problems. *ESAIM Math. Model. Numer. Anal.*, 49(2):577–599, 2015.
- [6] S. Berrone and A. Borio. A residual *a posteriori* error estimate for the Virtual Element Method. *Math. Models Methods Appl. Sci.*, 27(8):1423–1458, 2017.
- [7] A. Cangiani, E. H. Georgoulis, T. Pryer, and O. J. Sutton. A posteriori error estimates for the virtual element method. *Numer. Math.*, May 2017.
- [8] Ph. Clément. Approximation by finite element functions using local regularization. *Rev. Française Automat. Informat. Recherche Opérationnelle Sér. RAIRO Analyse Numérique*, 9(R-2):77–84, 1975.
- [9] D. Copeland, U. Langer, and D. Pusch. From the boundary element domain decomposition methods to local Trefftz finite element methods on polyhedral meshes. In *Domain decomposition methods in science and engineering XVIII*, volume 70 of *Lect. Notes Comput. Sci. Eng.*, pages 315–322. Springer, Berlin Heidelberg, 2009.
- [10] M. S. Floater. Generalized barycentric coordinates and applications. *Acta Numer.*, 24:161–214, 2015.
- [11] L. Formaggia and S. Perotto. New anisotropic a priori error estimates. *Numer. Math.*, 89(4):641–667, 2001.

- [12] L. Formaggia and S. Perotto. Anisotropic error estimates for elliptic problems. *Numer. Math.*, 94(1):67–92, 2003.
- [13] E. H. Georgoulis, E. Hall, and P. Houston. Discontinuous Galerkin methods for advection-diffusion-reaction problems on anisotropically refined meshes. *SIAM J. Sci. Comput.*, 30(1):246–271, 2007/08.
- [14] C. Hofreither, U. Langer, and S. Weißer. Convection adapted BEM-based FEM. *ZAMM - Z. Angew. Math. Mech.*, 96(12):1467–1481, 2016.
- [15] W. Huang. Mathematical principles of anisotropic mesh adaptation. *Commun. Comput. Phys.*, 1(2):276–310, 2006.
- [16] W. Huang, L. Kamenski, and J. Lang. A new anisotropic mesh adaptation method based upon hierarchical a posteriori error estimates. *J. Comput. Phys.*, 229(6):2179–2198, 2010.
- [17] P. Joshi, M. Meyer, T. DeRose, B. Green, and T. Sanocki. Harmonic coordinates for character articulation. *ACM Trans. Graph.*, 26(3):71.1–71.9, 2007.
- [18] G. Kunert. An a posteriori residual error estimator for the finite element method on anisotropic tetrahedral meshes. *Numer. Math.*, 86(3):471–490, 2000.
- [19] A. Loseille and F. Alauzet. Continuous mesh framework part I: well-posed continuous interpolation error. *SIAM J. Numer. Anal.*, 49(1):38–60, 2011.
- [20] S. Rjasanow and S. Weißer. Higher order BEM-based FEM on polygonal meshes. *SIAM J. Numer. Anal.*, 50(5):2357–2378, 2012.
- [21] S. Rjasanow and S. Weißer. FEM with Trefftz trial functions on polyhedral elements. *J. Comput. Appl. Math.*, 263:202–217, 2014.
- [22] R. Schneider. *A Review of Anisotropic Refinement Methods for Triangular Meshes in FEM*, pages 133–152. Springer Berlin Heidelberg, Berlin, Heidelberg, 2013.
- [23] L. R. Scott and S. Zhang. Finite element interpolation of nonsmooth functions satisfying boundary conditions. *Math. Comp.*, 54(190):483–493, 1990.
- [24] N. Sukumar and A. Tabarraei. Conforming polygonal finite elements. *Internat. J. Numer. Methods Engrg.*, 61(12):2045–2066, 2004.
- [25] R. Verfürth. *A review of a posteriori error estimation and adaptive mesh-refinement techniques*. Wiley-Teubner, 1996.
- [26] S. Weißer. Residual error estimate for BEM-based FEM on polygonal meshes. *Numer. Math.*, 118(4):765–788, 2011.
- [27] S. Weißer. Arbitrary order Trefftz-like basis functions on polygonal meshes and realization in BEM-based FEM. *Comput. Math. Appl.*, 67(7):1390–1406, 2014.
- [28] S. Weißer. Residual based error estimate and quasi-interpolation on polygonal meshes for high order BEM-based FEM. *Comput. Math. Appl.*, 73(2):187–202, 2017.
- [29] S. Weißer and T. Wick. The dual-weighted residual estimator realized on polygonal meshes. *Comput. Methods Appl. Math.*, 2017. (to appear).

STEFFEN WEISSER, DEPARTMENT OF MATHEMATICS, SAARLAND UNIVERSITY, 66041 SAARBRÜCKEN, GERMANY

E-mail address: weisser@num.uni-sb.de